

MOL #114231

## Title page

### **S29434, a quinone reductase 2 inhibitor: main biochemical and cellular characterization**

Jean A. Boutin<sup>1,\*</sup>, Frederic Bouillaud<sup>2</sup>, Elzbieta Janda<sup>3</sup>, István Gacsalyi<sup>4,\*\*</sup>, Gérald Guillaumet<sup>5</sup>, Etienne C. Hirsch<sup>6</sup>, Daniel A. Kane<sup>7</sup>, Françoise Nepveu<sup>8</sup>, Karine Reybier<sup>8</sup>, Philippe Dupuis<sup>9</sup>, Marc Bertrand<sup>10</sup>, Monivan Chhour<sup>8</sup>, Thierry Le Diguarher<sup>10</sup>, Mathias Antoine<sup>1</sup>, Karen Brebner<sup>7</sup>, Hervé Da Costa<sup>5,11</sup>, Pierre Ducrot<sup>1</sup>, Adeline Giganti<sup>1</sup>, Vishal Giri Goswami<sup>12</sup>, Hala Guedouari<sup>2</sup>, Patrick P. Michel<sup>6</sup>, Aakash Patel<sup>12</sup>, Jérôme Paysant<sup>13</sup>, Johann Stojko<sup>1</sup>, Marie-Claude Viaud-Massuard<sup>11</sup>, Gilles Ferry<sup>1</sup>

<sup>1</sup> Pôle d'Expertise Biotechnologie, Chimie & Biologie, Institut de Recherches SERVIER, 78290 Croissy-sur-Seine, France

<sup>2</sup> Institut Cochin, INSERM U1016, CNRS-UMR8104, Université Paris Descartes 75014 Paris, France

<sup>3</sup> Department of Health Sciences, Magna Graecia University, 88100 Catanzaro, Italy

<sup>4</sup> Egis Pharmaceuticals PLC, 1165 Budapest, Hungary.

<sup>5</sup> Institut de Chimie Organique et Analytique (ICOA), Université d'Orléans, UMR CNRS 7311, 45067 Orléans Cedex 2, France

<sup>6</sup> Institut du Cerveau et de la Moelle épinière, ICM, Inserm U 1127, CNRS UMR 7225, Sorbonne Université, F-75013, Paris, France

<sup>7</sup> Departments of Human Kinetics (DK) and Psychology (KB), St. Francis Xavier University, Antigonish, NS, Canada

<sup>8</sup> UMR 152 Pharma-Dev, Université de Toulouse, IRD, UPS, 31062 Toulouse, France

<sup>9</sup> EUROFINS-CEREP SA, 86600 Celle L'Evescault, France

<sup>10</sup> Technologie Servier, Orléans, France

<sup>11</sup> CNRS-UMR 7292 « GICC Innovation Moléculaire et Thérapeutique », Université de Tours, 37200 Tours, France

<sup>12</sup> Oxygen Healthcare Pvt Ltd, 382213 Ahmedabad, Gujarat, India

<sup>13</sup> Pôle d'Innovation Thérapeutique de Cardiologie, Institut de Recherches SERVIER, 92150, Suresnes, France

\*: present address Institut de Recherches Internationales Servier, 92150 – Suresnes

\*\* : present address : ATRC Aurigon Ltd., Budapest, Hungary

**MOL #114231**

**Running title page:**

**Running title:** Quinone reductase 2 inhibitor: S29434

**Corresponding author:**

\*Jean A. Boutin, Institut de Recherches Internationales Servier, 50 rue Carnot, 92284

Suresnes France

Telephone : +33(0)155724400

Email : [jean.boutin@servier.com](mailto:jean.boutin@servier.com)

**Abbreviations:** BNAH: *N*-benzylidihydronicotinamide; CLQ: chloroquine;; MPP+: 1-methyl-4-phenylpyridinium; MPTP: 1-methyl-4-phényl-1,2,3,6-tetrahydropyridine;; NRH: *N*-ribosylidihydronicotinamide; Psf: permeability surface filter ; Pst: permeability surface total; QR1: NAD(P)H dehydrogenase (quinone 1), EC 1.6.5.2; QR2: quinone reductase 2 or ribosylidihydronicotinamide dehydrogenase (quinone), formerly E.C. 1.10.99.2 now E.C. 1.10.5.1; ROS: reactive oxygen species; S29434: [2-(2-methoxy-5*H*-1,4b,9-triaza(indeno[2,1-*a*]inden-10-yl)ethyl)-2-furamide.

- Number of text pages: 31
- Number of tables: 1
- Number of figures: 13
- Number of references: 81
- Words in Abstract: 192
- Words in Introduction: 677
- Words in Discussion: 1491

**MOL #114231**

**Abstract:** Quinone reductase 2 (QR2, E.C. 1.10.5.1) is an enzyme with a feature that has attracted attention for several decades: in standard conditions, instead of recognizing NAD(P)H as an electron donor, it recognizes putative metabolites of NADH such as *N*-methyl- and *N*-ribosyl-dihydronicotinamide. QR2 has been particularly associated with reactive oxygen species and memory, strongly suggesting a link among QR2 (as a possible key element in pro-oxidation), autophagy, and neurodegeneration. In molecular and cellular pharmacology, understanding physiopathological associations can be difficult because of a lack of specific and powerful tools. Here we present a thorough description of the potent, nanomolar inhibitor S29434 ( $IC_{50} = 5$  to  $16$  nM) of QR2 at different organizational levels. We provide full detailed syntheses; describe its co-crystallization with and behavior at QR2 on a millisecond timeline; show that it penetrates cell membranes and inhibits QR2-mediated ROS production within the  $100$  nM range; and describe its actions in several *in vivo* models, and lack of actions in various ROS-producing systems. The inhibitor is fairly stable *in vivo*, penetrates cells, specifically inhibits QR2, and shows activities that suggest a key role for this enzyme in different pathological conditions including neurodegenerative diseases.

## Introduction

Quinone reductases, described as early as 1954 in peas, are pyridine nucleotide–dependent enzymes involved in the detoxification of natural quinones (Wosilait and Nason, 1954). Conover and Ernster (1960) first described the reference quinone reductase enzyme, initially designated as DT-diaphorase, in mammals. In the 1990s, another quinone reductase was cloned: quinone reductase 2 (QR2 or NQO2), with an unusual history (Zhao et al., 1997). The initial description indicated that QR2 was a strict analogue of quinone reductase 1 (a.k.a., DT-diaphorase, or NAD(P)H dehydrogenase (quinone 1), QR1, NQO1, E.C. 1.6.5.2), with similar properties. Later findings revealed, however, that it was quite different. Research in the 1960s identified QR2 as the only reductase using non-canonical co-substrates such as *N*-ribosyl- and *N*-methyl-dihyronicotinamide and para-quinones as substrates (Liao and Williams-Ashman, 1961; Liao et al., 1962), but not NADH or NADPH (Zhao et al., 1997; Ferry et al., 2010). Later, Talalay and colleagues cloned and crystallized QR2 (Zhao et al., 1997), but its physiologic role and specificity were poorly documented and understood, except that it recognized non-quinone compounds such as CB1954 as a substrate (Wu et al., 1997). This finding was the basis of efforts to develop CB1954 as a prodrug with interesting cytotoxic properties (Knox et al., 2003). QR2 has been implicated in effects distantly related to quinone metabolism, such as antimalarial action (Kwiek et al., 2004; Cassagnes et al., 2017), the AMPA-signaling pathway (Rappaport et al., 2015), paraquat-mediated toxicity (Janda et al., 2013; 2015), oxidative stress sensing (Leung and Shilton, 2013), and oocyte maturation (Chen et al., 2017).

In the search for the melatonin *MT3* binding site, described by Duncan et al. (1988) and our team (Paul et al., 1999), we found that the binding site was, in fact, in QR2 (Nosjean et al., 2000), see also discussion in Boutin & Ferry (2018). A screen of about 20,000 compounds from our library, comprising natural products such as flavonoids (Boutin et al., 2005), added

## MOL #114231

further candidates to the list of QR2 inhibitors. Already on this list were resveratrol (Buryanovskyy et al., 2004), tacrine (den Braver-Sewradj et al., 2017), chloroquine (CLQ) (Kwiek et al., 2004), dabigatran (a prescription thrombin inhibitor; Michaelis et al., 2012), and tetracyclic compounds (Boussard et al., 2006). Some products of quinone reduction are fairly unstable, especially in the absence of conjugating system(s), so the reaction products (quinols) may spontaneously yield back the original quinones in the presence of oxygen. Similar quinone cycling was described for QR1 (Bindoli et al., 1990; Nutter et al., 1992; Bian et al., 2017). Without the cellular conjugating capacities that neutralize the process by conjugating the quinol (*e.g.*, menadiol) with glucuronic acid (Kappus and Sies, 1981; Bolton et al., 2000; Nishiyama et al., 2010), the by-product of this futile cycle is the production of reactive oxygen species (ROS). Because electron paramagnetic resonance spectroscopy (EPR) can detect ROS generation (Reybier et al., 2011), we used this method to show that under some conditions, the pro-oxidant property of QR2 can be confirmed and measured.

Many organs and cells express QR2 (Nosjean et al., 2001), where it might have a key role in several pathological conditions. Given this potential, we assessed the specificity of the QR2 inhibitor S29434 and its actions in different contexts, adding to the already available data to consolidate its use as an established QR2 inhibitor tool. The present paper gives the full description of the characteristics of S29434. Despite several publications on this inhibitor, no report has described its synthesis, specificity for alternative enzymes or receptors, or characteristics of its stability in living systems. Thus, we generated as much information as possible about S29434 to make its use more appropriate for QR2 pharmacology. Here we cover its most important characteristics, from its chemistry and molecular and cellular pharmacology to its specificity for other ROS-generating systems and its *in vivo* activities. These data illustrate that S29434 or unknown metabolites reach QR2 and inhibit this enzyme

**MOL #114231**

*in situ*. Furthermore, its specificity seems to be limited to QR2, making this compound a valuable tool for understanding the role of QR2 in multiple scenarios, even *in vivo*.

MOL #114231

## Materials and Methods

**Chemical syntheses.** S29434 synthesis has never been published. Two different paths were explored for its synthesis. Both are summarized in **Fig. 1 & 2**. The synthetic routes are given in full details in the supplementary materials, as well as the various steps permitting to obtain the compounds are detailed in the **Supplementary data 1**. The final analyses of the product obtained with the second route are available as **Supplemental Data 1** (spectral analyses of compounds 3, 4 and S29434 obtained by the first synthetic route). All data obtained (analytical, spectral, biophysical) on the compound were consistent with its structure. S29434 was obtained with purity above 99% as adjudged by LC-MS and NMR (see Supplementary analytical Data),. Analytical details of the second route **Supplementary Figure S2** is also given as **Supplementary Data 2, 3, 4, 5, 6 and 7**.

**QR2 inhibition measurements.** The potency of S29434 was measured in standard kinetic assays. Briefly, QR2 enzymatic activity was measured under FAD saturation using substrate (menadione) and 100  $\mu$ M co-substrate BNAH or NRH. An oxidoreduction reaction was performed at 25 °C in a Tris-HCl 50 mM, pH 8.5, FAD 500 nM, octyl-glucopyranoside 1 mM, dimethylsulfoxide (DMSO) 5% buffer. Enzymatic kinetics measured the decrease in co-substrate absorbance corresponding to its oxidation. This reaction was followed either at 350 nm (BNAH) or 340 nm (NRH) on a FLUOstar 384-well plate reader (BMG, Offenburg, Germany). The slope of absorbance decrease was determined using FLUOstar Optima software (BMG) and expressed in units of optic density (UDO).s-1 then in M.s-1 using the Beer-Lambert law. This measurement was next corrected from its corresponding non-enzymatic (spontaneous) oxidation rate measured in the absence of enzyme, which corresponds to the specific maximum-activity oxidoreduction reaction. For the inhibitory hQR2 enzymatic activity assay, S29434 was used in the range of 50 pM to 5  $\mu$ M. The inhibitory concentration 50 % ( $IC_{50}$ ) and the inhibition percentage of co-substrate oxidation

**MOL #114231**

were determined using the PRISM program (GraphPad Software Inc., San Diego, CA, USA). These experiments were conducted over 50 times (inhibition, **Fig. 3A**) or in triplicate (**Fig. 3B**).

**Binding kinetics of S29434 and resveratrol to QR2 FADox (oxidized FAD).** Transient kinetics were measured at 25 °C (S29434) or 4 °C (resveratrol) with a SFM-300 stopped-flow mixer fitted with a FC-15 cell and coupled to a MOS-200 M rapid spectrophotometer equipped with a 150 W Xe–Hg lamp (Bio-Logic Science Instruments, Seyssinet-Pariset, France). Typical mixing dead time was 2.6 ms. QR2 tryptophans were excited at 295 nm to minimize photobleaching and excitation of tyrosines. Fluorescence emission was recorded using a 320-nm cutoff filter combined with a UG11 band-pass filter to block S29434 fluorescence. Binding experiments were performed under pseudo-first-order conditions by mixing an equal volume (75 µl) of QR2 and ligand in Tris–HCl 50 mM, β-octyl-D-glucopyranoside 1 mM, DMSO 5%, pH 8.5. QR2 monomer concentration after mixing was 1 µM. Fluorescence traces were first analyzed individually with the BioKine software (Bio-Logic, v4.80) as the sum of up to two exponential terms, as described by equation 1, with n being the number of exponentials, ai the amplitude of the ith exponential, kobsi the rate constant of the ith exponential, c the trace end point, and bt accounting for the slow linear drift caused by photobleaching. **Fig. 5** was generated with Prism (GraphPad, v7.03).

$$y = \left( \sum_{i=1}^n a_i e^{(-k_{\text{obs}i} t)} \right) + bt + c \quad (1)$$

The kobs values were plotted against ligand concentration. When a linear increase of kobs was observed, data were fitted to equation 2 describing a one-step binding mechanism, using Prism (GraphPad, v7.03).

$$k_{\text{obs}} = k_f[\text{ligand}] + k_{-1} \quad (2)$$

MOL #114231

**Specificity tests. General specificity.** Most of the tests were subcontracted to Eurofins. All experimental details can be found online on their site ([www.eurofinsdiscoveryservices.com](http://www.eurofinsdiscoveryservices.com)).

**Specificity tests. Kinases.** The panel of kinases for screening is available from Eurofins (ExpressDiversityKinase). It comprises 46 different kinases chosen to cover a maximal structural diversity among this large family of over 500 different enzymes. S29434 was tested at 100 nM on the enzymatic activity of all the kinases using a standard radiometric assay.

**Specificity tests Sirtuin experiments.** The use of this original technology has been reported in a technical note by Agilent (see [https://www.agilent.com/cs/library/applications/5990-9345en\\_lo.pdf](https://www.agilent.com/cs/library/applications/5990-9345en_lo.pdf)). In brief, recombinant sirtuin 1 (SIRT1) was produced in *E. coli* and purified. The non-acetylated and acetylated Foxo-3 substrates (hFoxo-3a-290-K(Ac): Ac-DSPSQLS-K(Ac)-WPGSPTS-NH<sub>2</sub>) were synthesized by GENEPEP SA (Saint-Jean-de-Védas, France). Deacetylase reactions were carried out in reaction buffer (Tris-HCl 50 mM, NaCl 137 mM, KCl 2.7 mM, MgCl<sub>2</sub> 1 mM, bovine serum albumin 0.05%, TCEp 1 mM, NAD<sup>+</sup> 0.8 mM) and 20 nM SIRT1 for 30 min at room temperature. The reaction was initiated by the addition of peptide substrate and quenched by the addition of 2% formic acid. The transitions of peptides detection: substrate: (excitation at 829.1 nm; emission at 544.6 nm) and product (excitation at 808.4 nm; emission at 544.5 nm) were detected.

**Specificity tests. NAD(P)H oxidase experiments.** This enzyme activity was measured using the lucigenin assay as described by Sasaki et al. (2013) and by Kuribayashi et al. (2008). This assay was adapted to the U937 cell line as biological source.

**ROS production in acellular and cellular experiments using electron paramagnetic resonance (EPR).** 5,5'-dimethyl-1-pyrroline *N*-oxide (DMPO) were purchased from Interchim (Montluçon, France). Menadione, adrenochrome, 3,3'-methylene-bis(4-hydroxycoumarin) (dicoumarol), NADH, and PBS were purchased from Sigma-Aldrich-Fluka

**MOL #114231**

Co. (Saint Quentin Fallavier, France). BNAH was purchased from TCI Europe (Zwijndrecht, Belgium). NRH was custom synthesized by O2h (Ahmedabad, India). DMSO was purchased from Fisher (UK, Loughborough). The DMPO stock solution (1 M) was prepared in water and stored at -80 °C until required. The inhibitors (S29434 and dicoumarol) were prepared as 1 mM solutions in DMSO and diluted in PBS to yield 0.2 mM. The substrates and co-substrates stock solutions were prepared in DMSO. Experiments on pure enzyme (QR1 or QR2) were performed with demineralized (18 M $\Omega$ ) and deaerated water containing tris(hydroxymethyl)amino-methane 50 mM and  $\beta$ -octyl-glucoside 1 mM, final pH 8.5. The EPR spectra were recorded immediately after mixing the pure enzyme with the inhibitor when needed (dicoumarol or S29434), DMPO (final concentration 125 mM), the co-substrate (NADH or NADPH for QR1 and NRH or BNAH for QR2, final concentration 3 mM) and finally the quinone (menadione, 125  $\mu$ M). Naïve Chinese Hamster Ovary cells (CHO-k1-NT) with basal expression of QR1 and QR2 and cell lines overexpressing QR1 (CHO-k1-QR1) or overexpressing QR2 (CHO-k1-QR2) were custom-made and purchased from Vectalys (Ramonville, France) (Cassagnes et al., 2015). The experiments were performed on  $5 \cdot 10^6$  cells suspended in a final volume of 400  $\mu$ l. EPR spectra were obtained at X-band and at room temperature on a Bruker EMX-8/2.7 (9.86 GHz) equipped with a high-sensitivity cavity (4119/HS 0205) and a gaussmeter (Bruker, Wissembourg, France). The analyses were performed with a flat quartz cell FZKI160-5 X 0.3 mm (Magnettech, Berlin, Germany). WINEPR and SIMFONIA software programs (Bruker) were used for EPR data processing and spectrum computer simulation. Typical scanning parameters were as follows: scan number, 5; modulation amplitude, 1 G; modulation frequency, 100 kHz; microwave power, 1 mW; sweep width, 100 G; sweep time, 41.94 s; time constant, 20.48 ms; and magnetic field 3465–3560 G. The intensities of the EPR signals were evaluated by measuring the amplitude peak to peak of the second line.

**MOL #114231**

**Liver and brain mitochondrial respiration.** The animal experimentation component of the studies was conducted with the approval of the local Animal Care and Use Committee and according to the applicable guidelines of the CNRS (<http://www.cnrs.fr/infoslabos/reglementation/euthanasie2.htm>). Rats (male, 150 g) were sacrificed by cervical dislocation followed by decapitation (fast bleeding). The liver and brain were quickly removed and placed in ice-cold mitochondria isolation buffer (sucrose 300 mM, Tris 10 mM, EGTA 1 mM, pH 7.4). Mitochondria were prepared by differential centrifugation, and the final mitochondrial pellet was resuspended in isolation buffer (20–80 mg/mL). Mitochondria were resuspended in 5 mL of mitochondrial respiration buffer (KCl 100 mM, sucrose 40 mM, TES 10 mM, MgCl<sub>2</sub> 5 mM, EGTA 1 mM, 5 mM phosphate, fatty acid-free bovine serum albumin 0.4 %, pH 7.2), and this suspension was distributed in each of the two chambers (2 mL final volume) of the Oxygraph 2K (Oroboros Instruments, Innsbrück, Austria). Temperature was set to 25 °C. Respiration was initiated with addition of glutamate and malate (5 mM each), and a fully stimulated phosphorylating state 3 was obtained by addition of 1.25 mM ADP. Increasing amounts of the S29434 were added to one chamber using 1,000 × concentrated working solutions in DMSO, and simultaneously the same volume (2 µl) of DMSO was added in the other chamber. For the liver experiments, 6 experiments, in 3 different days, with different mitochondria preparations were used. For the brain experiments, it was 3 different preparation that were used.

**Muscle mitochondrial respiration.** With the exception of Amplex Red Ultra (Life Technologies) and BNAH (see above), all chemicals and reagents were purchased from Sigma-Aldrich. Male Wistar rats were purchased from Charles River Laboratories, Inc. (Montréal, QC) and acclimated for approximately 2 weeks in the Animal Care Facility at St. Francis Xavier University (Canada). During the acclimation period, the rats were housed in

**MOL #114231**

pairs in standard cages with a plastic tunnel to provide environmental enrichment. All rats had access to standard rat chow and water, ad libitum. The room in which the rats were housed was maintained at 20 °C/22 °C and 40%/60% relative humidity and on a reversed 12-h light/dark cycle. Approval was granted by the institutional Animal Care Committee at St. Francis Xavier University prior to commencing the study, in accordance with guidelines of the Canadian Council on Animal Care guidelines. Variations of the permeabilized myofiber preparation are published elsewhere (Kuznetsov et al., 2008; Perry et al., 2011; Pesta and Gnaiger, 2012; Perry et al., 2013). In brief, immediately following euthanasia with sodium pentobarbital, two cuts were made on the right gastrocnemius muscle of each animal. Red (i.e., oxidative) portions of the gastrocnemius were extracted and placed in ice-cold buffer X, consisting of (in mM): 50 MES, 7.23 K<sub>2</sub>EGTA, 2.77 CaK<sub>2</sub>EGTA, 20 imidazole, 0.5 DTT, 20 taurine, 5.7 ATP, 14.3 phosphocreatine, and 6.56 MgCl<sub>2</sub>·6H<sub>2</sub>O (pH 7.1). Four fiber bundles from each gastrocnemius section were separated along the longitudinal axis, using needle tipped forceps (Fine Science Tools, Inc., Vancouver, CB, Canada) in ice-cold buffer X under magnification (Discovery V8, Carl Zeiss, Oberkochen, Germany). Following dissection, fiber bundles were placed in vials containing saponin (50 µg/mL) dissolved in 2.0 mL of buffer X. These vials were then placed on a nutating mixer (VWR International, Radnor, PA, USA) and kept at 4 °C for 30 min. After permeabilization, fiber bundles were transferred to a wash buffer solution, MiR05, consisting of (in mM): 20 taurine, 0.5 EGTA, 3 MgCl<sub>2</sub>, 60 K-lactobionate, 10 KH<sub>2</sub>PO<sub>4</sub>, 20 HEPES, 110 sucrose, 20 creatine, 1 g/L fatty acid-free bovine serum albumin, pH 7.1. Fiber bundles remained in MiR05 for approximately 15 min with regular inversion on the nutating mixer until experimentation, after which the samples were placed into the Oxygraph-2k (Oroboros). Blebbistatin was included in the permeabilization buffer, wash buffer, and assay to inhibit spontaneous contraction of muscle fibers (Perry et al., 2011; Perry et al., 2013). Substrate-dependent respiratory oxygen consumption was measured

**MOL #114231**

with the Oxygraph 2K (Oroboros). H<sub>2</sub>O<sub>2</sub> production was monitored in permeabilized rat red gastrocnemius muscle fibers simultaneously with respirometry using an amperometric add-on LED module to the Oroboros Oxygraph-2k. Prior to the first substrate addition of the respirometric protocol, 10 μM Amplex Red Ultra, 5 U/mL superoxide dismutase, and 1 U/mL horseradish peroxidase were added to the oxygraph chambers containing the fibers. H<sub>2</sub>O<sub>2</sub> calibration experiments were performed under the same parameters used for experimental data collection. The relationship between H<sub>2</sub>O<sub>2</sub> and fluorescence intensity was linear to at least 0.7 μM. Next the following were added, in order: 4 mM malate, 0.2 mM octanoylcarnitine, 5 mM ADP, 20 mM L-lactate, 5 mM NAD<sup>+</sup>, 5 mM pyruvate, and 10 μM UK-5099, and 10 mM glutamate was then added to test glutamate oxidation. Then, 10 mM succinate, 1 μM auranofin (thioredoxin reductase inhibitor), and 100 μM carmustine (BCNU; inhibitor of thioredoxin and glutathione reductases) were added to the chambers consecutively to inhibit the H<sub>2</sub>O<sub>2</sub> scavenging systems mitochondria. Finally, H<sub>2</sub>O<sub>2</sub> was titrated to internally calibrate the resorufin signal for H<sub>2</sub>O<sub>2</sub>. Following conclusion of the respirometry experiments, fibers were placed directly into water to clear out any remaining substrates in the cytosol. After 5 min, fiber bundles were then placed in a clean dry Eppendorf tube and freeze-dried using Labconco® FreeZone1. Following freeze-drying for 5 h, fiber bundles were weighed on a Mettler Toledo® Excellence Plus XP6 Ultra-Microbalance.

Results represent means ± SD; n = 4. A two-way, repeated measures ANOVA was completed for each oxygen flux and hydrogen peroxide production to identify any interaction among the three groups of exercise and histamine receptor antagonists, exercise only, and control. This step was followed by a one-way ANOVA with repeated measures (Bonferroni post hoc analysis) to examine differences between different substrate additions. Data analysis was completed using Prism 7 (GraphPad). The α-level for statistical significance was set at 0.05.

**MOL #114231**

**Measurement of mitochondrial ROS levels by flow cytometry in cells.** MitoSox (Thermo Fisher ScientificLife Tech., Molecular probes, Waltham, MA, USA) was used to measure mitochondrial superoxide levels in cells by flow cytometry. HepG2 were a kind gift from Dr. Eugenio Arcidiacono (University Magna Graecia, Catanzaro, Italy), were cultured in high-glucose (4.5 g/L) Dulbecco's modified essential medium (DMEM), as described (Lascala et al., 2018). U373 cells were cultured in low-glucose DMEM. Both types of DMEM were supplemented with 10 % fetal bovine serum (FBS), 1 % penicillin and streptomycin solution (Pen-Strep) and 1 % glutamine, all from Carlo Erba srl (Milan, Italy). HepG2 and U373 cells seeded on 24-well plates at the density  $80 \times 10^3$  and  $60 \times 10^3$  per well, respectively, 2 days before starting treatments. Cells were exposed to S29434 or vehicle (DMSO) for 6, 18 and 24 h before the end of the experiment. Next, the cells were washed with pre-warmed serum-free DMEM (high and low-glucose, depending on the cell type) and then incubated with MitoSox (2.5  $\mu$ M, 15 min) diluted in DMEM as above. The experiment was finished by washing the cells twice with pre-warmed phosphate-buffer saline followed by trypsin-mediated detachment of cells and flow cytometry analysis according to a previously published protocols (Janda et al., 2013)

**Transient silencing of QR2 expression and autophagy assay in hepatic cells.** HepG2 cells, were cultured as described above. Cells were seeded on 12-well plates one day before transfection at a density of 30,000  $\text{cm}^{-2}$ . Non-silencing or control (Ctrl) siRNA (All-stars) and a set of human QR2-targeting siRNA were purchased from Qiagen (Hilden, Germany). Transfection of HepG2 cells was performed using Lipofectamine 2000 (L2000, Life Technologies, Invitrogen, Monza MB, Italy) and Optimem (Life Technologies, Invitrogen) according to the manufacturer's instructions. Briefly, 360 pmol siRNA QR2 or control siRNA and 18  $\mu$ l of L2000 were mixed and incubated in 600  $\mu$ l of Optimem for 15–20 min at room temperature. Each well containing HepG2 cells in 500  $\mu$ l of serum-free medium was overlaid

## MOL #114231

with 100  $\mu$ l of siRNA-Lipofectamine complexes and incubated in a cell-culture incubator. After 5 h, the medium was changed for DMEM supplemented with FBS without Pen-Strep. At 24 h later, the cells were treated with S29434 or DMSO for 24 h in regular medium with Pen-Strep. CLQ 25  $\mu$ M was added 3 h before the end of the experiment to half of the samples. The cells were lysed, and the lysates were run on 12% SDS-PAGE gels and assayed for LC3 and QR2 expression by western blotting, as previously described (Janda et al., 2015). The antibodies were polyclonal rabbit anti-LC3A/B (MBL, Enzo Life Sciences, Farmingdale, NY, USA) used at 1:2000, anti-glyceraldehyde-3-phosphate dehydrogenase (Santa Cruz Biotech, Dallas, TX, USA) used at 1:500 and anti-QR2 (Sigma-Aldrich) used at 1:1000.

**Testing S29434 against neuronal degeneration in vitro.** Animals were housed, handled, and taken care of in accordance with recommendations of the Guide for the Care and Use of Laboratory Animals of the National Institutes of Health (NIH Publication no. 85-23, revised 1996) and the European Union Council Directives (2010/63/EU). Experimental procedures were authorized by the ethical committee on animal experiments (Comité Charles Darwin #5). Cultures were prepared from the ventral midbrain of Wistar rat embryos at gestational age 15.5 days (Janvier LABS, Le Genest-St.-Isle, France). Dissociated cells in suspension obtained by mechanical trituration of midbrain tissue pieces were seeded at a density of  $1.2\text{--}1.5 \times 10^5$  cells/cm<sup>2</sup> onto Nunc 48-well multi-dish plates precoated with 1 mg/mL polyethylenimine diluted in borate buffer, pH 8.3, as previously described (Toulorge et al., 2011). In some experiments, the cultures were maintained in N5 medium supplemented with 5 mM glucose, 5 % horse serum, and 0.5 % fetal calf serum, except for the first 3 days *in vitro*, when the concentration of fetal calf serum was set at 2.5 % to favor initial culture maturation (Guerreiro et al., 2008). In the other experiments, we used a chemically defined serum-free medium consisting of equal volumes of Dulbecco's minimal essential medium and Ham's F12 nutrient mixture (DMEM/F12, Life Technologies, Invitrogen), supplemented with 10

**MOL #114231**

$\mu\text{g/mL}$  insulin, 30 mM glucose, and 100 IU/mL Pen-Strep (Troadek et al., 2001). Dopamine neurons were detected by tyrosine hydroxylase immunofluorescence staining using procedures previously described (Toulorge et al., 2011). These neurons represented approximately 2-3% of the total number of neuronal cells present in these cultures after plating. The cultures, fixed for 12 min using 4% formaldehyde in Dulbecco's phosphate-buffered saline (PBS), were washed twice with PBS before an incubation step at 4 °C for 24 - 72 h with primary antibodies. A monoclonal anti- tyrosine hydroxylase antibody diluted 1/5000 (ImmunoStar, Inc., Hudson, WI, USA) or a polyclonal anti- tyrosine hydroxylase antibody diluted 1/1000 (US Biologicals, Salem, MA, USA) was used to assess survival of dopamine neurons. Cell counting was performed with a Nikon TE 2000 inverted microscope (Nikon, Champigny-sur-Marne, France) at 200 time magnification, using a 20  $\times$  objective matched with a 10  $\times$  ocular. The number of tyrosine hydroxylase+ neurons in each culture well was estimated after counting visual fields distributed along the x- and y-axes. The functional integrity and synaptic function of dopamine neurons were evaluated by their ability to accumulate [ $^3\text{H}$ ]-dopamine (50 nM; 40 Ci/mmol; PerkinElmer, Courtaboeuf, France), as previously described (Guerreiro et al., 2008). When using N5 medium supplemented with serum, dopamine neurons in culture degenerate spontaneously and progressively during the maturation process of these cultures (Toulorge et al., 2011). Thus, in this setting, pharmacological treatments were initiated immediately after plating and were then renewed daily after replacing a fraction (two thirds) of culture medium. Dopamine cell survival was assessed in 9 days in vitro cultures, i.e., at a stage where about 70 % of dopamine neurons have already died (Toulorge et al., 2011). Some sets of cultures were treated with veratridine (0.8  $\mu\text{M}$ ), a depolarizing agent used as a positive control for neuroprotection in this setting (Salthun-Lassalle et al., 2004). Treatments with the mitochondrial toxin  $\text{MPP}^+$  (1-methyl-4-phenylpyridinium) were performed in cultures in which the spontaneous death process was

## MOL #114231

prevented by supplementing the N5 medium with a depolarizing concentration of  $K^+$  (30 mM) in the presence of 1  $\mu$ M of the *N*-methyl-D-aspartate receptor antagonist dizocilpine ([5R,10S]-[1]-5-methyl-10,11-dihydro-5*H*-dibenzo[*a,d*]cyclohepten-5,10-imine, a.k.a. MK-801), as previously described (Salthun-Lassalle et al., 2004). Note that this treatment did not interfere with the neurotoxic effects of  $MPP^+$ .  $MPP^+$  was applied to midbrain cultures between 4 and 6 days in culture, whereas protective treatments were added after 2 days in vitro culture and renewed thereafter until fixation of the cultures at 6 days in culture. Finally, oxidative stress-mediated dopamine cell death was achieved by placing the cultures in a defined serum-free DMEM/F12 medium containing 1.5  $\mu$ M of ferrous iron (Troadek et al., 2001). The antimetabolic compound ARA-c (1.5  $\mu$ M) was added to the cultures after plating to prevent glial cell proliferation. Dopamine cell survival was assessed at 5 days in culture in these conditions. Experimental values expressed as mean  $\pm$  SEM were derived from triplicates of three independent experiments. Data were analyzed using the SigmaPlot 12.5 software (Systat Software Inc, San Jose, CA, USA) with one-way analysis of variance (ANOVA) followed the Student–Newman–Keuls post hoc test for all pairwise comparisons.

**Object recognition in mice.** Experiments were performed in a quiet, dimly lit room in a dark Plexiglas chamber (L  $\times$  W  $\times$  H: 25  $\times$  35  $\times$  25 cm). On the day before the test day (day 0, familiarization phase), the animals were allowed to explore the test apparatus for 2.5 min. Twenty-four hours later (day 1, acquisition phase), after a 30-min pretreatment time after drug treatment (1 and 15 mg/kg, i.p.), each test animal was placed in the middle of the test box from the previous day, and the 5-min acquisition trial was begun. In the first trial, mice were allowed to explore two identical objects (10 sec per object within a total 5-min period). During test time, the exploration time (ET) was measured with a stopwatch. ET is defined as direct, active olfactory exploration of objects 1 and 2. In general, it consists of nosing and sniffing of the edge and the top, as well as approaching and crossing the line approximately 1

**MOL #114231**

cm around the objects. Posturing and mounting are not included in measures of investigation. On day 2 (24 h later, retention phase), a new object and a familiar object were placed in the test box, and the animals were replaced in the box for 4 min and ET measured again. Discrimination index = [Exploration time of new object in seconds (N) – Exploration time of familiar object in seconds (F)]/[Exploration time of new object in seconds (N) + Familiar object exploration time in seconds (F)] = [N-F]/[N+F]. A thorough description of these methods can be found in previous publications (Ennaceur and Delacour, 1988; Bartolini et al., 1996; Bevins and Besheer, 2006). For in vivo data, one-way ANOVA was performed (followed by Dunnett's multiple comparisons test) for the DI data.

## Results

*Chemistry.* S29434 was synthesized by Guillaumet and colleagues in the late 1990s as a compound to explore the melatonergic system(s). We characterized it as an interesting tool for QR2 studies after we discovered that *MT3*, the unconventional melatonin binding site we and others described (Duncan et al., 1988; Paul et al., 1999), was indeed in QR2 (Nosjean et al., 2000). The first synthesis, as is typical, aimed at producing several examples of tetracyclic chemicals that could be assimilated into two indolic structures fused together. The goal at that stage was to document the chemical series, of which S29434 was the most potent. The route led to tens of milligrams of material and was not meant to yield greater quantity. The synthetic route is summarized in **Fig. 1**. The second synthesis scheme was intended to rationalize the yields of each step, even if alternative synthetic steps had to be substituted in the original protocols, as summarized in **Fig. 2**. This alternative route was meant to deliver gram amounts of the compound. Full details of the synthetic routes are given as supplementary data. Crucially, the final product, used in most of the experiments presented here, is 99% pure, based on LC-MS and NMR spectra data (**Supplementary data**). The mass spectrometry data as well as the NMR data confirmed the structure of the final product.

*Inhibition of QR2.* Various reports show that depending on the substrate/co-substrate couples used to measure the catalytic activity of QR2, the recorded  $IC_{50}$  values range from 1 to 40 nM (Table 1). We stabilized our system in a standard configuration (see materials and methods section) for all the internal needs for screening of this enzyme (S29434 was the reference compound) and identified an  $IC_{50}$  of  $16 \pm 3.2$  nM (mean  $\pm$  S.D.,  $n = 51$ ). The considerable amount of data accumulated on this material render this information quite robust, at least when using the human cloned enzyme, BNAH as co-substrate, and menadione as substrate. A typical sigmoid curve of the concentration/activity relationship is presented in **Fig. 3A**. We

**MOL #114231**

also present a comparison of S29434 inhibition of the enzyme catalytic activity while using BNAH, a synthetic co-substrate, or NRH, a natural candidate co-substrate of QR2 (**Fig. 3B**). With the natural co-substrate, the inhibition curve is shifted slightly leftward, from an  $IC_{50}$  of  $17 \pm 3$  nM in the presence of BNAH to  $5 \pm 1$  nM with NRH (mean  $\pm$  S.D.). Nevertheless, the use of BNAH is recommended because the compound is commercially available and slightly more robust than its ribosylated counterpart (Boutin et al., 2005). S29434 is a competitive inhibitor, as reported previously (Mailliet et al, 2005; Ferry et al., 2010; Pegan et al, 2011).

*Inhibitor specificity: Standard panel of molecular targets* (Eurofins-CEREP profiles). We first checked the specificity of the inhibitor S29434 for possible off-target activities (from the QR2 perspective). First, we assessed its activity in a series of standard assays designed to evaluate its behavior against a selection of receptors and enzymes (see, for example, Millan et al., 2012). All tests were done in duplicate, independently, at two concentrations: 100 nM and 10  $\mu$ M. With one exception, the results indicated no capacity of S29434 to inhibit binding at or activity of the selected targets, even at high concentrations ( $>10$   $\mu$ M) (data not shown). The notable exception was that S29434 could displace binding of 2-iodomelatonin at the melatonin receptor MT2, showing an affinity of 0.14  $\mu$ M. This result is not surprising given that S29434 was initially synthesized as part of a melatonin receptor agonist discovery process. Finally, S29434 showed no cytotoxic activities towards several standard cancer cell lines (Caco-2, HCT116, HT-29, and L1210) up to 10 mM, based on MTT assays.

*Inhibitor specificity: Kinases*. Duncan et al. (2008) reported the toxicity of two casein kinase 2 inhibitors, TBBz (4,5,6,7-1H-tetrabromobenzimidazole) and DMAT (2-dimethylamino-4,5,6,7-tetrabromo-1H-benzimidazole), presumably because of their inhibition of QR2 catalytic activity. Similarly, Rix et al. (2007) reported that QR2 is the only non-kinase target of the BCR-ABL inhibitors imatinib and nilotinib. Thus, we assessed whether the QR2 inhibitor could inhibit one or several catalytic activities of a panel of kinases. Of the 46

**MOL #114231**

included kinases, no inhibition greater than 20% was recorded for S29434 at 100 nM (data not shown). Because of the high potency of S29434, no higher concentrations were tested.

*Inhibitor specificity: QR1.* The best candidate for possible specificity of S29434 would be QR1, the closest relative of QR2. We also wanted to confirm that dicoumarol, the standard QR1 inhibitor (Ernster et al., 1962) in wide use, could not inhibit QR2. Based on previous catalytic activity measurement comparisons between the two enzymes (Ferry et al., 2010), S29434 shows good selectivity for QR2 over QR1, with the reverse result for dicoumarol. In a new set of experiments (**Fig. 4**), we used EPR analysis and showed that S29434 at 10  $\mu$ M did not inhibit QR1, compared to full inhibition by dicoumarol. Indeed, S29434 clearly had no effect on the intensity of the EPR spectrum, as represented by the six-lined spectrum characteristic of the radical adduct [DMPO-CH<sub>3</sub>]<sup>•</sup>. This radical adduct originates from the spin trapping of <sup>•</sup>CH<sub>3</sub> formed by reaction of <sup>•</sup>OH (produced during the re-oxidation of menadiol) with DMSO.

*Inhibitor specificity: sirtuin.* Because of the link between sirtuin-mediated NAD degradation (Jiang et al., 2017) and QR2's use of a possible NADH catabolite, we sought to ensure that the inhibitor's activity did not lead to upstream inhibition of sirtuin, diminishing the availability of its co-substrate. Even at 10  $\mu$ M, S29434 did not inhibit sirtuin, whereas superoxide dismutase and diphenyleneiodonium chloride were potent inhibitors (not shown).

*Inhibitor specificity: NADPH oxidase.* In addition to mitochondria, a main cellular source of ROS production is NADPH oxidase (Sorce et al., 2017; Teixeira et al., 2017). Thus, we checked the capacity of S29434 to inhibit this family of enzymes, using the NADPH oxidase inhibitor diphenyleneiodonium. The reference compound led to a complete inhibition, but S29434 remained poorly active up to 10  $\mu$ M, at which point it began to inhibit about 20% of ROS production from those cells (**Supplemental Figure 3**).

## MOL #114231

*S29434/quinone reductase 2 characteristics: Binding kinetics.* Resveratrol has been described as a potent inhibitor of QR2 (Buryanovskyy et al., 2004) and thus might serve as a reference compound in some conditions. The binding of either S29434 or resveratrol leads to quenching of the intrinsic fluorescence of QR2 (FADox). We used pre-equilibrium stopped-flow spectroscopy to measure the real-time binding kinetics of the two compounds and compare their binding mechanisms (**Fig. 5**). Resveratrol binding kinetics were too fast at 25 °C, so we decreased the temperature to 4 °C to slow the rate. The results were consistent with a single-step binding mechanism, governed by an association rate constant  $k_1$  of  $19 \times 10^6 \text{ s}^{-1} \text{ M}^{-1}$  and a dissociation rate constant  $k_{-1}$  of  $27 \text{ s}^{-1}$ . A  $K_D$  estimate of 1.4  $\mu\text{M}$  was calculated from the ratio  $k_{-1}/k_1$ , which is in good agreement with the isothermal titration calorimetric data obtained on the same enzyme batch, yielding a  $K_D$  of 0.6  $\mu\text{M}$  at 25 °C (data not shown). In contrast, S29434 displayed slower but biphasic binding transients, consistent with a two-step binding mechanism involving a conformational change. Re-plotting the  $k_{\text{obs}}$  rate constants for the fast phase yielded a linear plot, diagnostic of a bimolecular association step, governed by a  $k_1$  of  $14 \times 10^6 \text{ s}^{-1} \text{ M}^{-1}$  and a dissociation rate constant  $k_{-1}$  of  $61 \text{ s}^{-1} \cdot \text{M}^{-1}$ . A  $K_D$  estimate for this encounter complex of 4.4  $\mu\text{M}$  can be calculated from the ratio  $k_{-1}/k_1$ . The observed rate of the slow phase was independent of S29434 concentration in the investigated range, staying close to  $30 \text{ s}^{-1}$ . This step therefore likely reflects a conformational rearrangement, either following binding (induced fit) or preceding it (conformational selection). These preliminary kinetic data strongly suggest the evolution of the binding mechanism from the low-affinity single-step binder resveratrol to the high-affinity two-step binder S29434. They also are in agreement with results from our mass spectrometry studies of the inhibitor/enzyme binding (Antoine et al., 2012).

*S29434/QR2 characteristics: Co-crystallization.* Through various collaborations, we generated co-crystals of S29434 in QR2 that we deposited in the Protein Data Bank

## MOL #114231

(www.rcsb.org) (Pegan et al., 2011; Gerard et al., 2018) including several unpublished crystals at 1.4 Å resolution (4QOD); however, the interactions and orientation of the compound in the crystal were not discussed in great detail. In brief, as shown in **Fig. 6**, the ligand S29434 fits deeply into a QR2 hydrophobic cavity (PDB: 3OX3), interacting with subunits A and B with its amido-furan side chains pointing toward the solvent. It makes  $\pi$ -edge interactions with Trp105 and Phe126,  $\pi$ - $\pi$  interactions with Phe178, and a water-mediated H-bond with Asn161. Additional  $\pi$ - $\pi$  interactions exist with co-factor FAD. Although the furan moiety makes an additional hydrophobic interaction with Ile194 from QR2, this part of the molecule also seems to hang out of the catalytic site. This feature potentially offers the possibility of modification of this part of the molecule with, for instance, a fluorophore moiety, producing associated properties, as it has been done for chromen-2-one derivatives as inhibitors of QR1 (Bian et al, 2017).

*Transit of S29434 across the cellular membrane and blood–brain barrier.* We next conducted a series of experiments to characterize the properties of S29434 in terms of pharmacokinetics and cellular penetration. Firstly, we measured the behavior of S29434 in an in cellulo blood–brain barrier model (Cechelli et al., 1999), based on co-cultures of bovine brain micro-vessel endothelial cells and rat astrocytes (Booher and Sensenbrenner, 1972) showing expression of the pGP efflux transporter. For this purpose, we measured the permeability surface total (PSt) (filter + collagen + cells) and the permeability surface filter (PSf) (filter + collagen without cells) expressed in milliliters per minute. These values were 4.58 cm/min and 3.78 cm/min, respectively. Therefore, the ratio PSt/PSf (permeability class) for S29434 was determined to be 121%, showing no barrier effect of the BBB cells compared with the filter+collagen alone, classifying S29434 as a high permeable compound (Cechelli et al., 1999). Secondly, S29434 was tested on the well-known Caco2 model, expressing the main efflux transporters present at the intestinal and the BB barriers (pGP, BCRP and MRP2). The

**MOL #114231**

apical to basolateral (A2B) apparent permeability ( $P_{app}$ ) was  $33 \times 10^{-6}$  cm/s (incubation concentration at  $20 \mu\text{M}$ ) corresponding also to a high permeable compound, in the same range of that of propranolol, the high passive permeability reference. The basolateral to apical (B2A) permeability was not quantified in these experiments but the high A2B permeability suggested no efflux transporter involvement.

*QR2 and ROS production.* QR2 activity can be followed by EPR (Reybier et al., 2011; Cassagnes et al., 2015). As noted, this functional assay is indirectly linked to the enzyme. Indeed, the reaction product, a quinol, has poor stability in standard conditions. In the presence of oxygen, the quinol is oxidized back into the original quinone, which in turn serves as substrate for the enzyme. The result is a futile cycle between the two chemical species with the concomitant production of ROS [see Reybier et al. (2011) for a complete discussion]. This process seems to occur in acellular as well as cellular contexts (Cassagnes et al., 2017). Here, we completed and supported these findings, showing by EPR spectroscopy that pure QR2 in the presence of its co-substrate (BNAH) produces ROS during catalytic activity (**Fig. 7**); S29434 inhibits this effect. Furthermore, under those experimental conditions, neither NADH nor NAD(P)H could substitute for BNAH. Under basal conditions (no substrate or co-substrate of QR2), very low levels of ROS were recorded.

*QR2 and ROS production: Mitochondrial respiration in liver and brain.* Because S29434 diminishes the ROS produced during the futile cycle between quinol and quinone in aerobic conditions (Reybier et al., 2011), we wanted to ensure that this effect did not result from direct interference of S29434 with ROS even though the compound is inactive in other ROS-generating systems (such as mitochondria). Our results confirmed that S29434 cannot trap hydroxyl radicals ( $\bullet\text{OH}$ ) produced via the Fenton reaction or superoxide radicals ( $\text{O}_2\bullet^-$ ) produced from crown ether and  $\text{KO}_2$  (not shown). We also tested another source of cellular ROS production: the mitochondria. To evaluate the mitochondrial effect of the drugs,

**MOL #114231**

mitochondrial respiration was settled with complex I substrates (glutamate/malate) and in phosphorylating conditions (1.25 mM ADP). The relative effect of increasing amounts of S29434 is indicated by the ratio of respiratory rate compound/solvent, with a value of 1 indicating a lack of effect. With this approach, S29434 produced no effect up to 10  $\mu$ M concentrations and revealed no statistically significant changes in respiratory rate with rat liver or rat brain mitochondria (**Fig. 8**). The system was validated with experiments with rotenone or oligomycin, two known inhibitors of the mitochondrial respiratory chain, with results similar to those reported in the literature (data not shown).

*QR2 and ROS production: Mitochondrial respiration in muscle.* The next step involved independent assessment of mitochondria in saponin-permeabilized rat gastrocnemius muscle fibers. As illustrated in **Fig. 9A**, the conditions resulted in no differences in respiration, confirming that neither BNAH nor S29434 had an effect in these samples. Likewise, BNAH and S29434 did not affect H<sub>2</sub>O<sub>2</sub> production (**Fig. 9B**). Expression of H<sub>2</sub>O<sub>2</sub> as a percentage of O<sub>2</sub> flux yielded a statistically significant difference between BNAH and BNAH + S29434 (**Fig. 9C**) in the absence of ADP only. This finding suggested that BNAH may increase mitochondrial H<sub>2</sub>O<sub>2</sub> in non-phosphorylating (i.e., State 4 or LEAK) conditions. However, because neither respiration nor H<sub>2</sub>O<sub>2</sub> alone was affected, a more plausible explanation is that the difference in proportional H<sub>2</sub>O<sub>2</sub> production is the result of non-mitochondrial sources of H<sub>2</sub>O<sub>2</sub> in the samples, and not of bulk O<sub>2</sub> flux.

*Effects of S29434 on cells. Nervous system cells.* S29434 was described as having a beneficial effect against paraquat-induced toxicity *in cellulo* and *in vivo* (Janda et al., 2013, 2015), suggesting a potential role of QR2 in Parkinson's disease. This finding prompted us to analyze its effect in models of neuronal degeneration *in cellulo*. Primary midbrain dopamine neurons in culture were established from fetal rat ventral midbrains. In this system, S29434 (up 100  $\mu$ M) did not reduce spontaneous loss of dopamine neurons in culture (**Fig. 10 A**),

**MOL #114231**

while the reference neuroprotective molecule, veratridine, efficiently rescued these cells. S29434 also failed to protect dopaminergic cells from iron-induced oxidative stress (with iron in the culture medium) caused by a Fenton-type reaction occurring spontaneously (**Fig. 10 B**). At 100  $\mu\text{M}$ , S29434 even tended to become slightly toxic. As expected, however, the chelation of iron with deferoxamine (10  $\mu\text{M}$ ) led to robust protection under these conditions. In contrast to these observations, S29434 showed concentration-dependent protective effects against the mitochondrial complex I inhibitor  $\text{MPP}^+$  (**Fig. 10C**). This effect was already present at 0.1  $\mu\text{M}$ , peaked at 1  $\mu\text{M}$ , and declined progressively between 10 and 100  $\mu\text{M}$ . Nicotine, used at 10  $\mu\text{M}$  as a positive control, also rescued dopamine cells. Because  $\text{MPP}^+$  is selectively taken up by the dopamine transporter to exert its selective toxicity towards dopamine neurons, we tested whether S29434 operated as an inhibitor of dopamine uptake. We thus performed this routine experiment according to details already published in our laboratory (Guerreiro et al., 2008). S29434 does not bind to the ad hoc transporter (not shown), a finding that strongly suggests that it blocks the intrinsic mechanism of  $\text{MPP}^+$  toxicity, not its transport.

*Effects of S29434 on cells. Autophagy.* Autophagy is a vesicle-mediated pathway that ensures recognition and transport of defective organelles and protein aggregates to lysosomes, where they are digested. We tested if S29434 could induce autophagy in human HepG2 cells, a cell line derived from liver, the organ with the highest level of QR2 expression (Nosjean et al., 2000). S29434 dose-dependently induced LC3-II, a marker of autophagy vesicles (**Fig. 11A**). Silencing of QR2 by more than 50% increased basal LC3-II levels and suppressed LC3-II induction by S29434. This result indicated that the autophagy response to this compound does not depend on its off-target effects but is directly mediated by QR2 inhibition (second panel in **Fig. 11A, B**). Of importance, LC3-II was further accumulated in S29434-treated cells when autophagy flux was blocked by the lysosomal inhibitor Clq, indicating true induction of

**MOL #114231**

autophagy by the QR2 inhibitor (**Fig. 11B**). Further details are given in **Supplementary Data 8**, including discussion of the whole blots. These data confirm that QR2 plays a role in regulation of autophagy. Oxidative stress and redox reactions have a strong impact on autophagy machinery (Janda et al., 2012; 2015). Because QR2 inhibition does not reduce basal ROS levels in HepG2 cells (**Fig. 12A**) or U373 astrocytes (**Fig. 12B**), however, the mechanism by which S29434 triggers autophagy should be mitochondrial ROS-independent and QR2-dependent, as suggested by above results (**Fig. 11A, B; Supplementary Data 8**).

*Effects of S29434 in vivo. Object recognition tests in CH3 wild-type mice.* An interplay between QR2 and memory has been reported (Brouillette and Quirion, 2008; Benoit et al., 2010; Rappaport et al., 2015). To further assess this relationship, we used the inhibitor S29434 in the object recognition test. The test trial with the new object was carried out 24 h after the acquisition trial with two identical objects. S29434 was given intraperitoneally, 30 min before the acquisition trial (1 and 15 mg/kg, respectively). **Fig. 13A** shows the discrimination index, where N is the time spent inspecting the new object and F is the time spent exploring the familiar object during the test trial. Both concentrations of S29434 led to an enhanced time of exploration of the unfamiliar object, although the effects of the two doses (1 and 15 mg/kg) did not differ. Under these circumstances and experimental conditions, the object recognition memory of wild-type mice is enhanced by a factor of ~16 by i.p. injection of S29434 over control mice performance in the same test. As reported for other models (Rappaport et al., 2015), this finding suggests that by inhibiting QR2, S29434 has a positive effect at least on this particular aspect of memory.

*In vivo considerations on S29434: Object recognition memory in the KO CH3QR2<sup>-/-</sup> mice.* The same experiments were carried out on KO CH3QR2<sup>-/-</sup> mice, and the results are presented in **Fig. 13B**. For QR2 KO animals, the results strongly reinforce the previous findings. Indeed, treated (1 or 15 mg/kg) and control animals did not differ, indicating that the product has no

**MOL #114231**

further effect on this parameter. Because the QR2 KO animals were genetically deficient in this enzyme only (Mailliet et al., 2004), the lack of S29434 activity strongly suggests that the compound is specific to QR2. Furthermore, we know that these animals did not lose their learning capacity compared to the wild-type mice, as demonstrated in several tests including the Morris water maze, object recognition, and rotarod performance test. They performed better than their wild-type counterparts on all of these tests (Benoit et al., 2010).

## Discussion

*General.* Molecular pharmacology is based on either the manipulation (including the mutagenesis) of targets or their inhibition/activation by synthetic or natural chemicals. A good example is certainly dicoumarol, the QR1 reference inhibitor. This compound has been widely used in the literature (over 2700 references), yet many of its off-target effects bias the interpretation of the data obtained [see discussion in Scott et al. (2011)]. To avoid a similar scenario with S29434, here we sought to fill in information gaps related to this compound, including assessments of its *in cellulo* and *in vivo* activity, stability, permeability, and overall specificity and to publish a clear synthesis method.

*Chemistry.* S29434 belongs to a family of flat tetracyclic compounds, some that we (Boussard et al., 2006) and others have described, e.g., cryptolepines (Onyeibor et al., 2005; Lavrado et al., 2008; Whittell et al., 2011) or other types of indolizino-indolones (Bhattacharya et al., 2001). Compounds that inhibit QR2 activity also have been reported, including pyrroloquinoline ammosamides (Reddy et al., 2011), indolequinones (Dufour et al, 2011; Yan et al, 2011) and furan-amidines (Alnabulsi et al., 2018). Because few, if any, have been characterized beyond their enzymatic test activities, we believe that the present report is noteworthy because it describes S29434 activity in different *in cellulo* and *in vivo* situations.

*Acellular behavior, specificity.* In an acellular system, S29434 is a potent inhibitor of QR2 activity ( $IC_{50} \sim 10$  nM). It marginally inhibits QR1, if at all. Furthermore, S29434 does not potently inhibit more than 100 other targets, with the sole exception of the melatonin receptor 2, for which it has a binding affinity in the micromolar range. Of course, the notion of specificity is limited to targets for which measures are available. It is not possible to know if S29434 will uniquely recognize QR2 among the protein products of the 26,000 genes in the human genome. The mechanism by which S29434 binds to and interacts with QR2 has been

## MOL #114231

described (Pegan et al., 2011; Antoine et al., 2012). Here, we add information about the way the compound occupies the catalytic site of the enzyme. We also identify ways to measure S29434's affinity for QR2, in complement with its capacity to inhibit it. These two notions (affinity for the enzyme and inhibition potency) are too often conflated, and it is important to distinguish them. Furthermore, the biophysical measure allowed us to evaluate how long the compound sits in the catalytic site, which can vary widely across a series of analogue compounds for a given enzyme, ranging from seconds to hours.

*Stability in vivo, membrane crossing.* S29434 is demonstrated here to be highly permeable on both an in vitro BBB model that express the pGP and on the Caco2 model expressing the 3 main efflux transporters present at both intestinal and BBB barriers (pGP, BCRP, MRP2); this suggests no efflux involvement even if not directly demonstrated by bi-directional experiments. It was already clear that S29434 could penetrate different types of primary or cultivated cells (Benoit et al., 2010; Janda et al., 2013; Chen et al., 2017). Even if an in vivo pharmacokinetic study would have help to determine the PK parameters such as T<sub>1/2</sub> or bioavailability, the fact that the compound was active in rodent models when administered by intraperitoneal route (Janda et al., 2015; Rappaport et al., 2015) demonstrate that at least sufficient *in vivo* brain exposures (level and duration) were reached in mammals. Nevertheless, it is clear for us that a complete assessment of the plasma stability, as well as a quantification of the part of the injected molecule that reaches the brain of an animal after intraperitoneal treatment would greatly help the future studies.

*Cellular aspects, ROS.* As noted, QR2 is closely linked with ROS production. Thus, our main goal was to ensure that S29434 was not a scavenger *per se* and that the reduction in ROS bursts in cellular experiments was the result of S29434 interference with QR2. Indeed, the results showed that S29434 can inhibit QR2-dependent production of ROS in various cell types, including hepatoma HepG2 cells, the astroglial cell line U373 (Janda et al., 2013), and

**MOL #114231**

primary dopaminergic neurons (Cassagnes et al., 2017). However, it does not alter basal cellular ROS levels when applied in the absence of exogenous QR2 activators. For example, we treated HepG2 and U373 cells with S29434 at 6, 18, and 24 h before measuring intracellular ROS levels with MitoSox, a fluorescent compound recognizing preferentially mitochondrial superoxide anion (Polster et al., 2014). MitoSox fluorescence was unaltered by S29434 at all experimental times in HepG2, but a nonspecific antioxidant, *N*-acetyl cysteine, statistically significantly reduced basal ROS levels (Fig. 12). Mitochondria are the main source of cellular ROS in physiological conditions. Thus, we conducted detailed studies on mitochondria from various organs to validate that in all conditions, S29434 did not inhibit this ROS production. Furthermore, S29434 did not inhibit NADPH oxidase or impair ROS produced from a Fenton-type reaction that exert toxicity neuronal cells. These data support that S29434 is specific to QR2.

*Cellular aspects, autophagy.* The autophagy pathway mitigates cellular damage from stress and toxic agents and plays an important role in ensuring basal protein and organelle turnover (Janda et al., 2012; Dagda et al., 2013). While studying the antioxidant effects of S29434 on paraquat-induced toxicity, we discovered that this compound has yet another property: the ability to restore basal autophagy in paraquat-treated astrocytes. In addition, S29434 induces autophagy in the absence of paraquat, a response mediated by a QR2-dependent mechanism in astrocytes (Janda et al., 2015). The data presented here indicate that the QR2-dependent mechanism of autophagy induction can be generalized to other cell types such as liver cells. Furthermore, we show that this effect does not correlate with any detectable modulation of ROS levels in liver cells, thus excluding a possible ROS-dependent basis of the pro-autophagic activity of S29434. The accumulation of LC3-II in the presence of CIQ is believed to result from a blockade of lysosome activity. It might depend in part, however, on the ability of the anti-malaria drug CIQ to bind and inhibit QR2 directly, although with poor affinity

**MOL #114231**

compared to S29434 (Kwiek et al., 2004; Leung and Shilton, 2015). Indeed, the direct effect of CIQ on QR2 is much weaker than its inhibitory effect on lysosomal digestion because LC3-II still accumulates when QR2 expression is reduced by siRNA (Fig. 11B, compare lines 1 and 4).

*Cellular aspects, neuronal cells.* MPP<sup>+</sup>, the active metabolite of MPTP, inhibits mitochondrial complex I. When delivered into mice, MPP<sup>+</sup> leads to a Parkinson-like syndrome. We know that QR2 does not recognize MPTP as a substrate; nevertheless, S29434 shows concentration-dependent protection in this model. Of interest, paraquat and MPP<sup>+</sup> are both parkinsonian toxins and share common toxicity mechanisms, including inhibition of mitochondrial complex I activity and dysregulation of autophagy (Dagda et al., 2013) and both compound effects are suppressed by a QR2 inhibitor..

*In vivo activity, ultimate specificity.* An ultimate proof of specificity is when enzyme activity is linked to a clear phenotypic outcome (e.g., effects on memory or certain types of memory) *in vivo*. Here we found that on an object recognition memory test, wild-type mice are sensitive to S29434. After treatment, the animals spent an enhanced period of time exploring the unfamiliar object compared to untreated mice, suggesting a role of QR2 in memory, in keeping with earlier findings (Harada et al., 2001; Benoit et al., 2011; Rappaport et al., 2015). Finally, in the same experiments in QR2 knockout mice, the compound shows no effect. Since the first suggestion of a memory effect (Brouillette and Quirion, 2008), other findings also have linked QR2 catalytic activity to suppression of several types of memory, potentially associated with dopaminergic neurons (McNab et al., 2009; Rossato et al., 2009; Nobili et al., 2017 see also review by D'Amelio et al. 2018).

Although we did not address S29434 activity in various models of inflammation, which is often linked to ROS production, the inhibitor does not influence Toll-like receptors or inflammasome signaling (Groß et al., 2016) as an activator or inhibitor (O. Gross, personal

**MOL #114231**

communication). Further work is needed to better understand a possible role of QR2 in inflammation responses.

In summary, S29434 is a powerful inhibitor of QR2 with an  $IC_{50}$  in the low nanomolar range (5 to 16, depending on the co-substrate used). It is specific to QR2 over a range of standard pharmacological targets, is fairly stable *in vivo*, and penetrates cells. The current findings do not guarantee specificity of S29434 but clearly delineate some of its actions, particularly in various models that help link its activities to its powerful inhibition of QR2. Several other inhibitors of QR2 have been described, such as resveratrol, melatonin, and some flavonoids, but they are non-specific, inhibiting many enzymes in many pathways; thus, using them to dissect a given pathway is untenable. As such, we believe that the present work lays a strong foundation for the pharmacological use of S29434 to evaluate specifically the role of QR2.

**MOL #114231**

**Acknowledgments:** JAB wishes to thank Dr. Hemal Soni (O2h, Ahmedabad, India) for his help in writing the second chemical part, San Francisco Edit for their help in editing and rewriting this manuscript, Mrs. Laure Allain for her daily help and finally Drs. Philippe Delagrangé (Servier, Croissy-sur-Seine, France), Nathaniel Gould & Kobi Rosenblum (Haifa, Israel) and Olaf Gross (München, Germany) for their intellectual contributions. E. Janda wishes to thank Dr. Concetta Martino (UMG Catanzaro, Italy) for technical assistance. E.C. Hirsch and P.P. Michel thank Cécile Bureau and Laetitia Da Costa for their technical help. Drs. D.A. Kane and K. Brebner thank Mackenzie Bell, Laura Davidson, and Helen Elizabeth Wallace for their technical assistance.

**MOL #114231**

**Authorship Contributions:**

Participated in research design: Bertrand, Bouillaud, Boutin, Ferry, Gacsalyi, Guillaumet, Hirsch, Janda, Kane, Le Diguarher, Nepveu, Reybier, Viaud-Massuard.

Conducted experiments: Antoine, Brebner, Chhour, Da Costa, Dupuis, Giganti, Goswani, Guerdouari, Janda, Michel, Patel, Paysant, Reybier, Stojko,

Performed data analysis: Antoine, Bertrand, Bouillaud, Boutin, Ducrot, Dupuis, Gacsalyi, Hirsch, Giganti, Janda, Kane, Le Diguarher, Nepveu, Paysant, Reybier, Stojko, Viaud-Massuard

Wrote or contributed to the writing of the manuscript: Antoine, Boutin, Bouillaud, Ducrot, Dupuis, Ferry, Gacsalyi, Guillaumet, Hirsch, Janda, Kane, Le Diguarher, Nepveu, Paysant, Reybier, Stojko,

## References

- Alnabulsi S, Hussein B, Santana E, Alsalahat I, Kadirvel M, Magwaza RN, Bryce RA, Schwalbe CH, Baldwin AG, Russo I, Stratford IJ, and Freeman S (2018) Evaluation of analogues of furan-amidines as inhibitors of NQO2. *Bioorg Med Chem Lett* **28**:1292–1297.
- Antoine M, Marcheteau E, Delagrangre P, Ferry G, and Boutin JA (2012) Characterization of cofactors, substrates and inhibitor binding to flavoenzyme quinone reductase 2 by automated supramolecular nano-electrospray ionization mass spectrometry. *Int J Mass Spectrom* **312**:87–96.
- Bartolini L, Casamenti F, and Pepeu G (1996) Aniracetam restores object recognition impaired by age, scopolamine, and nucleus basalis lesions. *Pharmacol Biochem Behav* **53**:277–283.
- Benoit CE, Bastianetto S, Brouillette J, Tse Y, Boutin JA, Delagrangre P, Wong T, Sarret P, and Quirion R (2010) Loss of quinone reductase 2 function selectively facilitates learning behaviors. *J Neurosci* **30**:12690–12700.
- Benoit CE, Rowe WB, Menard C, Sarret P, and Quirion R (2011) Genomic and proteomic strategies to identify novel targets potentially involved in learning and memory. *Trends Pharmacol Sci* **32**:43–52.
- Bevins RA and Besheer J (2006) Object recognition in rats and mice: A one-trial non-matching-to-sample learning task to study ‘recognition memory’. *Nat Protoc* **1**:1306–1311.
- Bhattacharya G, Su T-L, Chia C-M, and Chen K-T (2001) Synthesis and Autoxidation of New Tetracyclic 9 H,10 H -Indolizino[1,2- b ]indole-1-ones. *J Org Chem* **66**:426–432.
- Bian J, Li X, Xu L, Wang N, Qian X, You Q, and Zhang X (2017) Affinity-based small fluorescent probe for NAD(P)H: Quinone oxidoreductase 1 (NQO1). Design, synthesis and pharmacological evaluation. *Eur J Med Chem* **127**:828–839.
- Bindoli A, Rigobello MP, and Galzigna L (1990) Reduction of adrenochrome by rat liver and brain DT-diaphorase. *Free Radic Res Commun* **8**:295–298.
- Bolton JL, Trush MA, Penning TM, Dryhurst G, and Monks TJ (2000) Role of quinones in toxicology. *Chem Res Toxicol* **13**:135–160.
- Booher J and Sensenbrenner M (1972) Growth and cultivation of dissociated neurons and glial cells from embryonic chick, rat and human brain in flask cultures. *Neurobiology* **2**:97–105.
- Boussard MF, Truche S, Rousseau-Rojas A, Briss S, Descamps S, Droual M, Wierzbicki M, Ferry G, Audinot V, Delagrangre P, and Boutin JA (2006) New ligands at the melatonin binding site MT(3). *Eur J Med Chem* **41**:306–320.
- Boutin JA (2016) Quinone reductase 2 as a promising target of melatonin therapeutic actions. *Expert Opin Ther Targets*. **20**:303–317 doi: 10.1517/14728222.2016.1091882.
- Boutin JA, Chatelain-Egger F, Vella F, Delagrangre P, and Ferry G (2005) Quinone reductase 2 substrate specificity and inhibition pharmacology. *Chem Biol Interact* **151**:213–228.
- Boutin JA, and Ferry G (2018) Is there sufficient evidence that the melatonin binding site MT3 is quinone reductase 2? *J Pharmacol Exp Ther* **in press**. doi: 10.1124/jpet.118.253260.
- Brouillette J and Quirion R (2008) Transthyretin: A key gene involved in the maintenance of memory capacities during aging. *Neurobiol Aging* **29**:1721–1732.
- Buryanovskyy L, Fu Y, Boyd M, Ma Y, Hsieh T-c, Wu JM, and Zhang Z (2004) Crystal structure of quinone reductase 2 in complex with resveratrol. *Biochemistry* **43**:11417–11426.

**MOL #114231**

- Cassagnes LE, Perio P, Ferry G, Moulharat N, Antoine M, Gayon R, Boutin JA, Nepveu F, and Reybier K (2015) In cellulo monitoring of quinone reductase activity and reactive oxygen species production during the redox cycling of 1,2 and 1,4 quinones. *Free Radic Biol Med* **89**:126–134.
- Cassagnes LE, Rakotoarivelo N, Sirigu S, Perio P, Najahi E, Chavas LM, Thompson A, Gayon R, Ferry G, Boutin JA, Valentin A, Reybier K, and Nepveu F (2017) Role of Quinone Reductase 2 in the Antimalarial Properties of Indolone-Type Derivatives. *Molecules* **22**:E210.
- Cechelli R, Dehouck B, Descamps L, Fenart L, Buee-Scherrer V, Duhem C, Lundquist S, Rentfel L, Torpier G, and Dehouck MP (1999) In vitro model for evaluating drug transport across the blood-brain-barrier. *Adv Drug Deliv Rev* **36**:165–178.
- Chen D, Li X, Liu X, Liu X, Jiang X, Du J, Wang Q, Liang Y, and Ma W (2017) NQO2 inhibition relieves reactive oxygen species effects on mouse oocyte meiotic maturation and embryo development. *Biol Reprod* **97**:598–611.
- Conover TE and Ernster L (1960) Mitochondrial oxidation of extra-mitochondrial TPNH1 mediated by purified DT diaphorase. *Biochem Biophys Res Commun* **2**:26–30.
- D'Amelio M, Puglisi-Allegra S, and Mercuri N (2018) The role of dopaminergic midbrain in Alzheimer's disease: Translating basic science into clinical practice. *Pharmacol Res* **130**:414–419.
- Dagda RK, Das Banerjee T, and Janda E (2013) How Parkinsonian toxins dysregulate the autophagy machinery. *Int J Mol Sci* **14**:22163–22189.
- den Braver-Sewradj SP, den Braver MW, Toorneman RM, van Leeuwen S, Zhang Y, Dekker SJ, Vermeulen NPE, Commandeur JNM, and Vos JC (2017) Reduction and scavenging of chemically reactive drug metabolites by NAD(P)H: Quinone oxidoreductase 1 and NRH:quinone oxidoreductase 2 and variability in hepatic concentrations. *Chem Res Toxicol* **31**:116–126.
- Dufour M, Yan C, Siegel D, Colucci MA, Jenner M, Oldham NJ, Gomez J, Reigan P, Li Y, De Matteis CI, Ross D, Moody CJ (2011) mechanism-based inhibition of quinone reductase 2 (NQO2): selectivity for NQO2 over NQO1 and structural basis for flavoprotein inhibition. *ChemBioChem* **12**:1203-1208.
- Duncan JS, Gyenis L, Lenehan J, Bretner M, Graves LM, Haystead TA, and Litchfield DW (2008) An unbiased evaluation of CK2 inhibitors by chemoproteomics: Characterization of inhibitor effects on CK2 and identification of novel inhibitor targets. *Mol Cell Proteomics* **7**:1077–1088.
- Duncan MJ, Takahashi JS, and Dubocovich ML (1988) 2-[125I]iodomelatonin binding sites in hamster brain membranes: Pharmacological characteristics and regional distribution. *Endocrinology* **122**:1825–1833.
- Ennaceur A and Delacour J (1988) A new one-trial test for neurobiological studies of memory in rats. 1: Behavioral data. *Behav Brain Res* **31**:47–59.
- Ernster L, Danielson L, and LJUNGGREN M (1962) DT diaphorase. I. Purification from the soluble fraction of rat-liver cytoplasm, and properties. *Biochim Biophys Acta* **58**:171–188.
- Ferry G, Hecht S, Berger S, Moulharat N, Coge F, Guillaumet G, Leclerc V, Yous S, Delagrangé P, and Boutin JA (2010) Old and new inhibitors of quinone reductase 2. *Chem Biol Interact* **186**:103–109.
- Gerard CJJ, Ferry G, Vuillard LM, Boutin JA, Ferte N, Grossier R, Candoni N, and Veessler S (2018) A Chemical Library to Screen Protein and Protein–Ligand Crystallization Using a Versatile Microfluidic Platform. *Cryst Growth Des* **18**:5130–5137.
- Groß CJ, Mishra R, Schneider KS, Médard G, Wettmarshausen J, Dittlein DC, Shi H, Gorka O, Koenig P-A, Fromm S, Magnani G, Ćiković T, Hartjes L, Smollich J, Robertson AAB, Cooper MA, Schmidt-Supprian M, Schuster M, Schroder K, Broz P, Traidl-Hoffmann C,

**MOL #114231**

- Beutler B, Kuster B, Ruland J, Schneider S, Perocchi F, and Groß O (2016) K + Efflux-Independent NLRP3 Inflammasome Activation by Small Molecules Targeting Mitochondria. *Immunity* **45**:761–773.
- Guerreiro S, Toulorge D, Hirsch E, Marien M, Sokoloff P, and Michel PP (2008) Paraxanthine, the primary metabolite of caffeine, provides protection against dopaminergic cell death via stimulation of ryanodine receptor channels. *Mol Pharmacol* **74**:980–989.
- Harada S, Fujii C, Hayashi A, and Ohkoshi N (2001) An Association between Idiopathic Parkinson's Disease and Polymorphisms of Phase II Detoxification Enzymes: Glutathione S-Transferase M1 and Quinone Oxidoreductase 1 and 2. *Biochem Biophys Res Commun* **288**:887–892.
- Janda E, Isidoro C, Carresi C, and Mollace V (2012) Defective autophagy in Parkinson's disease: Role of oxidative stress. *Mol Neurobiol* **46**:639–661.
- Janda E, Lascala A, Carresi C, Parafati M, Aprigliano S, Russo V, Savoia C, Ziviani E, Musolino V, Morani F, Isidoro C, and Mollace V (2015) Parkinsonian toxin-induced oxidative stress inhibits basal autophagy in astrocytes via NQO2/quinone oxidoreductase 2: Implications for neuroprotection. *Autophagy* **11**:1063–1080.
- Janda E, Parafati M, Aprigliano S, Carresi C, Visalli V, Sacco I, Ventrice D, Mega T, Vadala N, Rinaldi S, Musolino V, Palma E, Gratteri S, Rotiroti D, and Mollace V (2013) The antidote effect of quinone oxidoreductase 2 inhibitor against paraquat-induced toxicity in vitro and in vivo. *Br J Pharmacol* **168**:46–59.
- Jiang Y, Liu J, Chen D, Yan L, and Zheng W (2017) Sirtuin Inhibition: Strategies, Inhibitors, and Therapeutic Potential. *Trends Pharmacol Sci* **38**:459–472.
- Kappus H and Sies H (1981) Toxic drug effects associated with oxygen metabolism: Redox cycling and lipid peroxidation. *Experientia* **37**:1233–1241.
- Knox RJ, Burke PJ, Chen S, and Kerr DJ (2003) CB 1954: From the Walker tumor to NQO2 and VDEPT. *Curr. Pharm. Des* **9**:2091–2104.
- Kuribayashi F, Tsuruta S, Yamazaki T, Nunoi H, Imajoh-Ohmi S, Kanegasaki S, and Nakamura M (2008) Cell adhesion markedly increases lucigenin-enhanced chemiluminescence of the phagocyte NADPH oxidase. *Genes Cells* **13**:1249–1256.
- Kuznetsov AV, Veksler V, Gellerich FN, Saks V, Margreiter R, and Kunz WS (2008) Analysis of mitochondrial function in situ in permeabilized muscle fibers, tissues and cells. *Nat Protoc* **3**:965–976.
- Kwiek JJ, Haystead TA, and Rudolph J (2004) Kinetic mechanism of quinone oxidoreductase 2 and its inhibition by the antimalarial quinolines. *Biochemistry* **43**:4538–4547.
- Lascala A, Martino C, Parafati M, Salerno R, Oliverio M, Pellegrino D, Mollace V, and Janda E (2018) Analysis of proautophagic activities of Citrus flavonoids in liver cells reveals the superiority of a natural polyphenol mixture over pure flavones. *J Nutr Biochem* **58**:119–130.
- Lavrado J, Paulo A, Gut J, Rosenthal PJ, and Moreira R (2008) Cryptolepine analogues containing basic aminoalkyl side-chains at C-11: Synthesis, antiplasmodial activity, and cytotoxicity. *Bioorg Med Chem Lett* **18**:1378–1381.
- Leung KK and Shilton BH (2013) Chloroquine binding reveals flavin redox switch function of quinone reductase 2. *J Biol. Chem.* **288**:11242–11251.
- Leung KK and Shilton BH (2015) Quinone reductase 2 is an adventitious target of protein kinase CK2 inhibitors TBBz (TBI) and DMAT. *Biochemistry* **54**:47–59.
- Liao S, Dulaney J, and Willaims-Ashman HG (1962) Purification and properties of a flavoprotein catalyzing the oxidation of reduced ribosyl nicotinamide. *J Biol Chem* **237**:2981–2987.

**MOL #114231**

- Liao S and Williams-Ashman HG (1961) Enzymatic oxidation of some non-phosphorylated derivatives of dihydronicotinamide. *Biochem Biophys Res Commun* **4**:208–213.
- Mailliet F, Ferry G, Vella F, Thiam K, Delagrang P, and Boutin JA (2004) Organs from mice deleted for NRH:quinone oxidoreductase 2 are deprived of the melatonin binding site MT3. *FEBS Lett* **578**:116–120.
- Mailliet F, Ferry G, Vella F, Berger S, Cogé F, Chomar P, Mallet C, Guening SP, Guillaumet G, Viaud-Massard MC, Yous S, Delagrang P, Boutin JA (2005) Characterization of melatonergic MT3 binding site as the NRH:quinone oxidoreductase 2 catalytic site. *Biochem Pharmacol* **71**:74–88.
- McNab F, Varrone A, Farde L, Jucaite A, Bystritsky P, Forsberg H, and Klingberg T (2009) Changes in Cortical Dopamine D1 Receptor Binding Associated with Cognitive Training. *Science* **323**:800–802.
- Michaelis S, Marais A, Schrey AK, Graebner OY, Schaudt C, Sefkow M, Kroll F, Dreger M, Glinski M, Koester H, Metternich R, and Fischer JJ (2012) Dabigatran and dabigatran ethyl ester: Potent inhibitors of ribosyl-dihydronicotinamide dehydrogenase (NQO2). *J Med Chem* **55**:3934–3944.
- Millan MJ, La Mannoury Cour C, Chanrion B, Dupuis DS, Di Cara B, Audinot V, Cussac D, Newman-Tancredi A, Kamal M, Boutin JA, Jockers R, Marin P, Bockaert J, Muller O, Dekeyne A, and Lavielle G (2012) S32212, a Novel Serotonin Type 2C Receptor Inverse Agonist/ 2-Adrenoceptor Antagonist and Potential Antidepressant: I. A Mechanistic Characterization. *J Pharmacol Exp Ther* **340**:750–764.
- Nishiyama T, Izawa T, Usami M, Ohnuma T, Ogura K, and Hiratsuka A (2010) Cooperation of NAD(P)H:quinone oxidoreductase 1 and UDP-glucuronosyltransferases reduces menadione cytotoxicity in HEK293 cells. *Biochem Biophys Res Commun* **394**:459–463.
- Nobili A, Latagliata EC, Viscomi MT, Cavallucci V, Cutuli D, Giacobuzzo G, Krashia P, Rizzo FR, Marino R, Federici M, Bartolo P de, Aversa D, Dell'Acqua MC, Cordella A, Sancandi M, Keller F, Petrosini L, Puglisi-Allegra S, Mercuri NB, Coccorello R, Berretta N, and D'Amelio M (2017) Dopamine neuronal loss contributes to memory and reward dysfunction in a model of Alzheimer's disease. *Nat Comm* **8**:14727.
- Nosjean O, Ferro M, Coge F, Beauverger P, Henlin JM, Lefoulon F, Fauchere JL, Delagrang P, Canet E, and Boutin JA (2000) Identification of the melatonin-binding site MT3 as the quinone reductase 2. *J Biol Chem* **275**:31311–31317.
- Nosjean O, Nicolas JP, Klupsch F, Delagrang P, Canet E, and Boutin JA (2001) Comparative pharmacological studies of melatonin receptors: MT1, MT2 and MT3/QR2. Tissue distribution of MT3/QR2. *Biochem Pharmacol* **61**:1369–1379.
- Nutter LM, Ngo EO, Fisher GR, and Gutierrez PL (1992) DNA strand scission and free radical production in menadione-treated cells. Correlation with cytotoxicity and role of NADPH quinone acceptor oxidoreductase. *J Biol Chem* **267**:2474–2479.
- Onyeibor O, Croft SL, Dodson HI, Feiz-Haddad M, Kendrick H, Millington NJ, Parapini S, Phillips RM, Seville S, Shnyder SD, Taramelli D, and Wright CW (2005) Synthesis of Some Cryptolepine Analogues, Assessment of Their Antimalarial and Cytotoxic Activities, and Consideration of Their Antimalarial Mode of Action. *J Med Chem* **48**:2701–2709.
- Paul P, Lahaye C, Delagrang P, Nicolas JP, Canet E, and Boutin JA (1999) Characterization of 2-[125I]iodomelatonin binding sites in Syrian hamster peripheral organs. *J Pharmacol. Exp Ther* **290**:334–340.
- Pegan SD, Sturdy M, Ferry G, Delagrang P, Boutin JA, and Mesecar AD (2011) X-ray structural studies of quinone reductase 2 nanomolar range inhibitors. *Protein Sci* **20**:1182–1195.

**MOL #114231**

- Perry CG, Kane DA, Lanza IR, and Neuffer PD (2013) Methods for assessing mitochondrial function in diabetes. *Diabetes* **62**:1041–1053.
- Perry CG, Kane DA, Lin CT, Kozy R, Cathey BL, Lark DS, Kane CL, Brophy PM, Gavin TP, Anderson EJ, and Neuffer PD (2011) Inhibiting myosin-ATPase reveals a dynamic range of mitochondrial respiratory control in skeletal muscle. *Biochem J* **437**:215–222.
- Pesta D and Gnaiger E (2012) High-resolution respirometry: OXPHOS protocols for human cells and permeabilized fibers from small biopsies of human muscle. *Methods Mol Biol* **810**:25–58.
- Polster BM, Nicholls DG, Ge SX, and Roelofs BA (2014) Use of potentiometric fluorophores in the measurement of mitochondrial reactive oxygen species. *Meth Enzymol* **547**:225–250.
- Rappaport AN, Jacob E, Sharma V, Inberg S, Elkobi A, Ounallah-Saad H, Pasmanik-Chor M, Edry E, and Rosenblum K (2015) Expression of Quinone Reductase-2 in the Cortex Is a Muscarinic Acetylcholine Receptor-Dependent Memory Consolidation Constraint. *J Neurosci* **35**:15568–15581.
- Reddy PVN, Jensen KC, Mesecar AD, Fanwick PE, and Cushman M (2011) Design, Synthesis, and Biological Evaluation of Potent Quinoline and Pyrroloquinoline Ammosamide Analogues as Inhibitors of Quinone Reductase 2. *J Med Chem* **55**:367–377.
- Reybier K, Perio P, Ferry G, Bouajila J, Delagrangé P, Boutin JA, and Nepveu F (2011) Insights into the redox cycle of human quinone reductase 2. *Free Radic Res* **45**:1184–1195.
- Rix U, Hantschel O, Durnberger G, Remsing Rix LL, Planyavsky M, Fernbach NV, Kaupé I, Bennett KL, Valent P, Colinge J, Kocher T, and Superti-Furga G (2007) Chemical proteomic profiles of the BCR-ABL inhibitors imatinib, nilotinib, and dasatinib reveal novel kinase and nonkinase targets. *Blood* **110**:4055–4063.
- Rossato JI, Bevilacqua LRM, Izquierdo I, Medina JH, and Cammarota M (2009) Dopamine Controls Persistence of Long-Term Memory Storage. *Science* **325**:1017–1020.
- Salthun-Lassalle B, Hirsch EC, Wolfart J, Ruberg M, and Michel PP (2004) Rescue of mesencephalic dopaminergic neurons in culture by low-level stimulation of voltage-gated sodium channels. *J Neurosci* **24**:5922–5930.
- Sasaki S, Yamada S, Iwamura M, and Kobayashi Y (2013) Specific detection of intramitochondrial superoxide produced by either cell activation or apoptosis by employing a newly developed cell-permeative lucigenin derivative, 10,10'-dimethyl-9,9'-biacridinium bis(monomethyl terephthalate). *Free Radic Biol Med* **65**:1005–1011.
- Scott KA, Barnes J, Whitehead RC, Stratford IJ, and Nolan KA (2011) Inhibitors of NQO1: Identification of compounds more potent than dicoumarol without associated off-target effects. *Biochem Pharmacol* **81**:355–363.
- Sorce S, Stocker R, Seredenina T, Holmdahl R, Aguzzi A, Chio A, Depaulis A, Heitz F, Olofsson P, Olsson T, Duveau V, Sanoudou D, Skosgater S, Vlahou A, Wasquel D, Krause K-H, and Jaquet V (2017) NADPH oxidases as drug targets and biomarkers in neurodegenerative diseases: What is the evidence? *Free Radic Biol Med* **112**:387–396.
- Teixeira G, Szyndralewicz C, Molango S, Carnesecchi S, Heitz F, Wiesel P, and Wood JM (2017) Therapeutic potential of NADPH oxidase 1/4 inhibitors. *Br J Pharmacol* **174**:1647–1669.
- Toulorge D, Guerreiro S, Hild A, Maskos U, Hirsch EC, and Michel PP (2011) Neuroprotection of midbrain dopamine neurons by nicotine is gated by cytoplasmic Ca<sup>2+</sup>. *FASEB J* **25**:2563–2573.
- Troade J-D, Marien M, Darios F, Hartmann A, Ruberg M, Colpaert F, and Michel PP (2001) Noradrenaline provides long-term protection to dopaminergic neurons by reducing oxidative stress. *J Neurochem* **79**:200–210.

**MOL #114231**

- Whittell LR, Batty KT, Wong RPM, Bolitho EM, Fox SA, Davis TME, and Murray PE (2011) Synthesis and antimalarial evaluation of novel isocryptolepine derivatives. *Bioorg Med Chem* **19**:7519–7525.
- Wosilait WD and Nason A (1954) Pyridine nucleotide-quinone reductase. I. Purification and properties of the enzyme from pea seeds. *J Biol Chem* **206**:255–270.
- Wu K, Knox R, Sun XZ, Joseph P, Jaiswal AK, Zhang D, Deng PS, and Chen S (1997) Catalytic properties of NAD(P)H:quinone oxidoreductase-2 (NQO2), a dihydronicotinamide riboside dependent oxidoreductase. *Arch Biochem Biophys* **347**:221–228.
- Yan C, Dufour M, Siegel D, Reigan P, Gomez J, Shieh B, Moodu CJ, Ross D (2011) Indolequinone inhibitors of NRH:quinone oxidoreductase 2. Characterization of the mechanism of inhibition in both cell-free and cellular systems. *Biochemistry* **50**:6678-6688.
- Zhao Q, Yang XL, Holtzclaw WD, and Talalay P (1997) Unexpected genetic and structural relationships of a long-forgotten flavoenzyme to NAD(P)H:quinone reductase (DT-diaphorase). *Proc Natl Acad Sci USA* **94**:1669–1674.

**MOL #114231**

**Footnote:**

E. Hirsch and P. Michel acknowledge the support of the funding programs “Investissements d’avenir” ANR-10-IAIHU-06 and “Investissements d’avenir” ANR-11-INBS-0011-NeurATRIS: Translational Research Infrastructure for Biotherapies in Neurosciences. This work benefited from equipment and services from the CELIS core facility (Institut du Cerveau et de la Moelle Epinière, Paris). Dr. D.A. Kane acknowledges support from the Canada Foundation for Innovation and the Natural Sciences and Engineering Research Council of Canada. Dr. E. Janda received financial support from Herbal and Antioxidant Derivatives *srl*, Bianco (RC), Italy and from FFARB 2017 (Basic Research Activities Fund).

MOL #114231

### Legends for figures

**Fig. 1: Schematic representation of the synthesis of S29434.** Note that the yields presented in the figure are not to be mistaken for the purity of the intermediary compound(s), which was usually above 95%.

**Fig. 2: Schematic representation of an alternate synthesis of S29434.** Note that the yield presented here is not to be taken for the purity of the final compound(s), which was usually above 95%.

**Fig. 3: QR2 inhibition by S29434.** **A)** Inhibition profile of S29434 on pure QR2. The pure enzyme (2 nM) was incubated with 100  $\mu$ M of BNAH and 100  $\mu$ M of menadione in a buffer consisting of 1 mM n-octyl-beta D-glucopyranoside in 50 mM Tris-HCl, pH 8.5, and 500 nM FAD. In the absence of enzyme, the reduction did not occur. **B)** Inhibition profile S29434 as a function of hQR2 co-substrate. IC<sub>50</sub> values were assessed in a standard enzymatic assay (Tris-HCl 50 mM, pH 8.5, FAD 500 nM, n-octyl-B-d-glucopyranoside 1 mM, DMSO 5%) consisting of 0.5 nM *E. coli*-expressed human QR2 preincubated with S29434 [50 pM–5  $\mu$ M], either BNAH (dashed line) or NRH (plain line) 100  $\mu$ M, and triggered by addition of menadione 100  $\mu$ M. Results are expressed as % inhibition of the control activities deduced from BNAH (350 nm) or NRH (340 nm) absorbance measurements. Each point of the curves represents the mean  $\pm$  standard deviations (S.D.) of three independent experiments.

**Fig. 4: Specificity of S29434 towards QR1. Comparison with dicoumarol.** ROS production recorded with purified QR1 (5  $\mu$ g/mL) in the presence of NADH (100  $\mu$ M) and menadione (100  $\mu$ M) following pre-incubation with buffer (control), S29434 (10  $\mu$ M), or

**MOL #114231**

dicoumarol (10  $\mu\text{M}$ ). The corresponding EPR spectra are presented on the right panels. The production of ROS was evaluated by the double integration of the EPR spectra obtained with DMPO (50 mM) as spin-trap. Histograms represent the intensity of the signals as mean  $\pm$  S.D. of three independent measures.

**Fig. 5: Binding kinetics of resveratrol and S29434 to QR2 (FADox).** **A–C)** Resveratrol. **D–F)** S29434. **A)** Fluorescence transients measured after mixing QR2 and resveratrol at 4  $^{\circ}\text{C}$ , final concentrations were 1  $\mu\text{M}$  and 8  $\mu\text{M}$ , respectively. **B)** Residuals of the mono-exponential fit. **C)** Re-plot of the  $k_{\text{obs}}$  values overlaid with the corresponding linear fit. **D)** Fluorescence transients measured after mixing QR2 and S29434 at 25  $^{\circ}\text{C}$ ; final concentrations were 1  $\mu\text{M}$  and 8  $\mu\text{M}$ , respectively. **E)** Residuals of the bi-exponential fit. **F)** Re-plot of the  $k_{\text{obs}}$  values for the fast (upper plot) and slow (lower plot) phases. The fast-phase plot is overlaid with the corresponding linear fit.

Panels **C** and **F** are box and whiskers graphs: The box extends from the 25th to 75th percentiles. The median is plotted as the line in the middle of the box. The whiskers go down to the smallest value and up to the largest. They were constructed from 6 replicates.

**Fig. 6: Co-crystallization of S29434 with QR2.** This co-crystallization of human QR2 with S29434 has been deposited in the PDB under the code PDB: 3OX3 (Pegan et al, 2011). **A)** QR2 molecular surface colored by lipophilicity (blue: hydrophilic regions; green: hydrophobic regions). Ligand S29434 (coral, space-filling model). **B)** Ligand S29434 binding cavity (orange: chain 1; pink: chain B; coral: ligand; lipophilic surface). **C)** Left: QR2/S29434 interactions; right: QR2/S29434 interactions with FAD (grey).

**Fig. 7: Effect of co-substrate and inhibitor on the QR2-dependent production of ROS.**

**MOL #114231**

*Left panel:* ROS production recorded with purified QR2 (25.6  $\mu\text{g/mL}$ ) and different co-substrates: BNAH, NADH, or NAD(P)H, in the presence or not of 20  $\mu\text{M}$  S29434. ROS production was evaluated by the double integration of the EPR spectra obtained with DMPO (50 mM) as spin-trap. The histograms represent the mean  $\pm$  S.D. of at least four independent measures. *Right panel:* A representative crude EPR spectrum recorded with BNAH or NADH and menadione is shown.

**Fig. 8: Effect of S29434 on respiration of rat liver and brain mitochondria.** Rat liver mitochondria (**A, B**) and rat brain mitochondria (**C, D**) oxygen consumption was measured simultaneously in the two chambers of the respirometer O2k ([www.oroboros.at](http://www.oroboros.at)). Successive additions are indicated below the x-axis (time). First (left to the vertical dotted line), we settled a fast respiring phosphorylating state by addition of substrates glutamate/malate (GM) and ADP. Then (right to the dotted line), four additions of increasing concentrations ( $10^{-7}$  to  $10^{-4}$  M) of S29434 were made (black line and empty dots) as a control, and the same volumes of solvent (DMSO) were added (grey line). **A, B:** mean value of the oxygen consumption rate [in pmol/(s. mg protein)]. \*  $p < 0.05$  with a paired t-test to compare the oxygen consumption rate with S29434 (100  $\mu\text{M}$ ) or solvent for the same period of time. Experiments were run 6 times on different rat liver preparations. **C, D:** ratio between the rates for S29434/solvent. \*\*  $p < 0.01$  with the Mann–Whitney rank test (<http://vassarstats.net/>) for the comparison of the ratio observed with S29434 at  $10^{-4}$  with each of the others comparable situations (ADP and no further addition, S29434  $10^{-7}$  to  $10^{-5}$  M). Experiments were run 3 times on different rat brain preparations.

MOL #114231

**Fig. 9: Effects of S29434 on mitochondrial respiration or H<sub>2</sub>O<sub>2</sub> production in permeabilized skeletal muscle.** Saponin-permeabilized rat red gastrocnemius skeletal muscle fibers were incubated in the following prior to assay: 100 μM BNAH, 30 μM S29434, 100 μM BNAH + 30 μM S29434, or control (vehicle: 18.75 μL DMSO). Subsequently, respiration was measured in all conditions (A), and H<sub>2</sub>O<sub>2</sub> in S29434 and BNAH + S29434 conditions (B). H<sub>2</sub>O<sub>2</sub> as a percentage of O<sub>2</sub> consumed was also calculated. Results represent means ± SD; n = 4. \*p < 0.05, \*\*p < 0.01, n = 7.

**Fig. 10: S29434 effects on neuronal cell cultures.** A) S29434 does not protect dopamine neurons that degenerate spontaneously in midbrain cultures maintained with serum-supplemented N5 medium. The effect of S29434 against cell death was tested at the concentrations indicated above. The reference compound is veratridine (VERA; 0.8 μM). \*p < 0.05 vs. corresponding controls. B) S29434 does not protect dopamine neurons that degenerate from oxidative stress in midbrain cultures maintained with a chemically defined medium containing catalytic iron. S29434 was tested at concentrations indicated above. The reference compound was deferoxamine (DESF; 10 μM). \*p < 0.05 vs. corresponding controls. C) S29434 protects dopamine neurons against MPP<sup>+</sup>-induced cell death. Survival of TH<sup>+</sup> neurons in midbrain cultures treated (open bars) or not with MPP<sup>+</sup> at a concentration of 3 μM. The effect of S29434 against MPP<sup>+</sup>-induced cell death was tested at concentrations indicated above. Reference compound is nicotine (Nic; 10 μM). \*p < 0.05 vs. corresponding controls.

**Fig. 11: Induction of autophagy by S29434 in HepG2 cells is QR2-dependent.** HepG2 cells were transfected with 100 μM siRNA against QR2 or non-targeting siRNA (negative

**MOL #114231**

control). The following day, cells were treated with S29434 (5 and 10  $\mu$ M) or vehicle (DMSO) for 24 h. **(B)** Lysosomal function inhibitor chloroquine (25  $\mu$ M) or vehicle (water) **(A)** was added to duplicate experimental points 2.5 h before the lysis and analysis of LC3 levels by western blot (SDS-PAGE 12%). Optical density (OD) relative to loading control (glyceraldehyde-3-phosphate dehydrogenase) was analyzed for LC3-II and normalized to control DMSO-treated cells for chloroquine-treated and untreated samples, separately.

**Fig. 12: S29434 has no effect on basal mitochondrial ROS levels in cells.** Subconfluent **A)** human hepatoma (HepG2) and **B)** astrocytoma (U373) cell lines were treated with S29434 (10  $\mu$ M), N-acetylcysteine (5 mM), or vehicle (DMSO) for 6, 18, and 24 h before analysis. ROS levels were determined by flow cytometry after staining with MitoSOX. The graphs show the mean  $\pm$  SEM from three independent experiments performed at least in triplicate. Statistical analysis two-way ANOVA, followed by Tukey post-test, time versus pharmacological treatment, 3 groups per 3 times, n = 3 or 4 samples each group, \*\*, p < 0.01 when compared to control at the same time point.

**Fig. 13: Effect of S29434 *in vivo* on object recognition memory.** **A)** Object recognition memory is enhanced by S29434 in wild-type mice. The test trial with the new object was carried out 24 h after the acquisition trial with two identical objects. S29434 was given intraperitoneally 30 min before the acquisition trial (1 and 15 mg/kg). The discrimination index (DI) is shown where N is the time spent inspecting the new object and F is the time spent exploring the familiar object during the test trial. Data are mean  $\pm$  SEM, n = 9–10/group. \*\*\* p < 0.001, one-way ANOVA followed by Dunnett's test vs. medium-treated control animals (0 mg/kg). **B)** Lack of effect of S29434 on object recognition memory in

**MOL #114231**

CH3QR2<sup>-/-</sup> mice. The test trial with the new object was carried out 24 h after the acquisition trial with two identical objects. S29434 was given intraperitoneally 30 min before the acquisition trial (1 and 15 mg/kg). The discrimination index (DI) is shown where N is the time spent inspecting the new object and F is the time spent exploring the familiar object during the test trial. Data are mean  $\pm$  SEM, n = 10/group. \*\* p < 0.01 one-way ANOVA followed by Dunnett's test vs. medium-treated control animals (0 mg/kg).

**Table 1: Summary of the IC<sub>50</sub> values from different laboratories and conditions with S29434**

Enzyme	Co-substrate	Substrate	Signal	IC <sub>50</sub> (nM) (mean ± SD)	References
h QR2 expressed in <i>E. coli</i>	BNAH (100 μM)	Menadione	Abs* 350 nm	16 ± 3.2	Present paper
h QR2 expressed in <i>E. coli</i>	NRH (100 μM)	Menadione	Abs* 340 nm	5 ± 1	Present paper
h QR2 expressed in <i>E. coli</i>	BNAH (100 μM)	Menadione	Abs* 350 nm	17 ± 3	Present paper
h QR2 expressed in CHO	BNAH (100 μM)	Menadione	Fluo** BNAH	14 ± 1	(Mailliet et al., 2005)
h QR2 expressed in CHO	BNAH (100 μM)	Menadione	Fluo** BNAH	14 ± 7	(Pegan et al., 2011)
h QR2 expressed in <i>E. coli</i>	NMeH (100 μM)	Menadione	Abs* 360 nm	2.4 ± 0.7	(Pegan et al., 2011)
h QR2 expressed in <i>E. coli</i>	NMeH (100 μM)	Formosan	Abs*** 612 nm	11 ± 2	(Pegan et al., 2011)
h QR2 expressed in insect cells	BNAH (100 μM)	Menadione	Fluo** BNAH	6.7 ± 0.7	(Ferry et al., 2010)
h QR2 expressed in insect cells	NRH (100 μM)	Menadione	Fluo** NRH	0.7 ± 0.1	(Ferry et al., 2010)
h QR2 expressed in insect cells	NRH (100 μM)	Coenzyme Q2	Fluo** NRH	5 ± 0.9	(Ferry et al., 2010)

Notes: \*Abs: absorbance assay; \*\*Fluo: fluorimetric assay; \*\*\*Absorbance of MTT

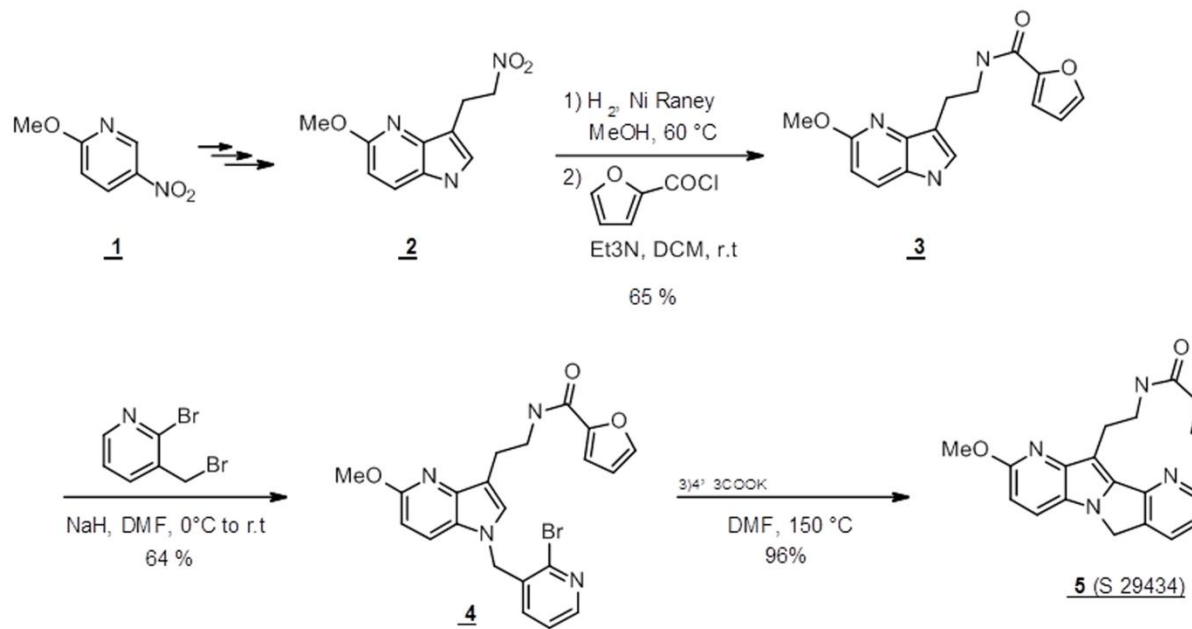


Figure 1

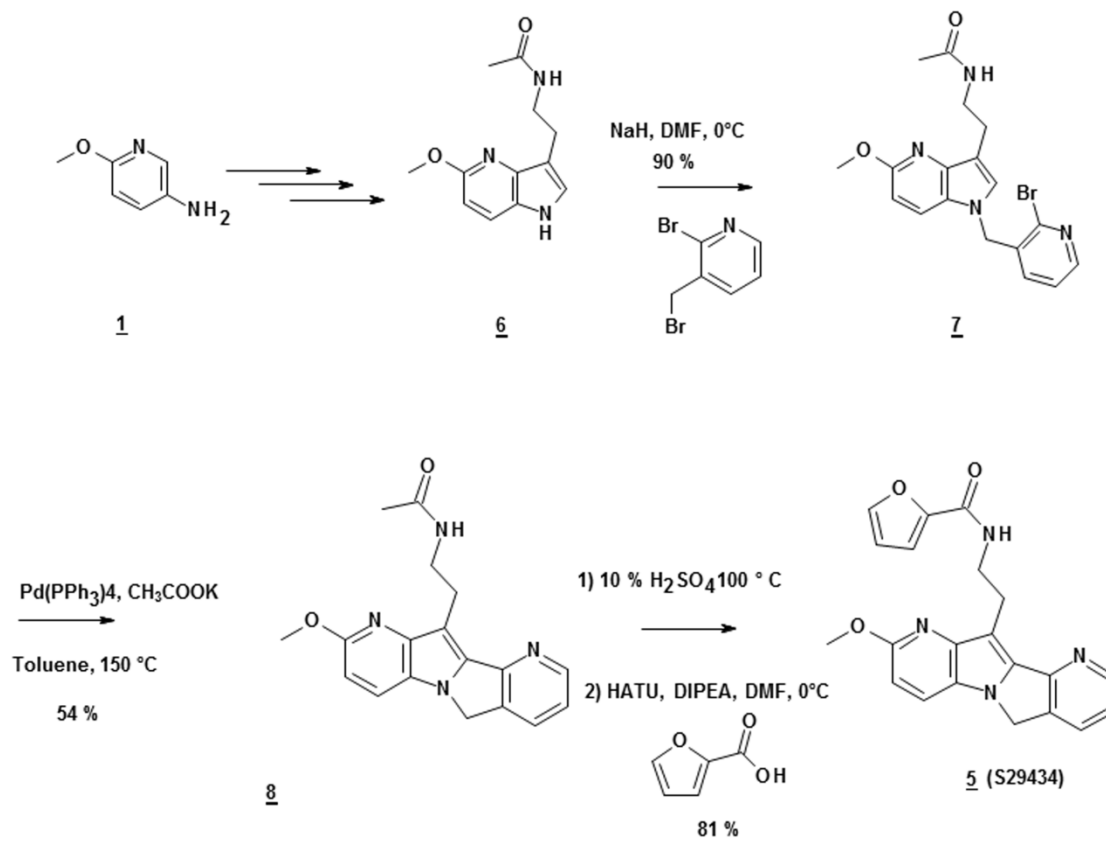


Figure 2

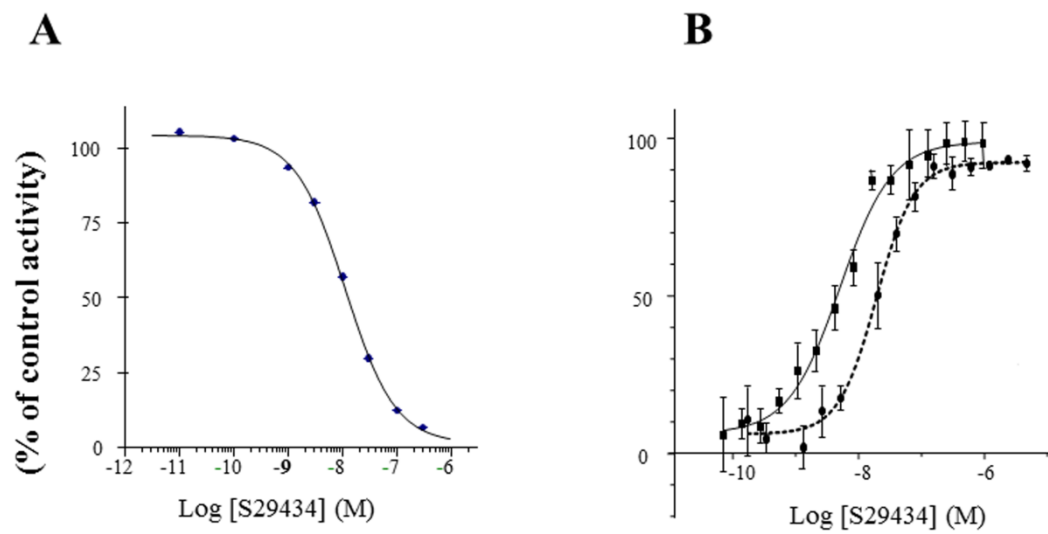


Figure 3

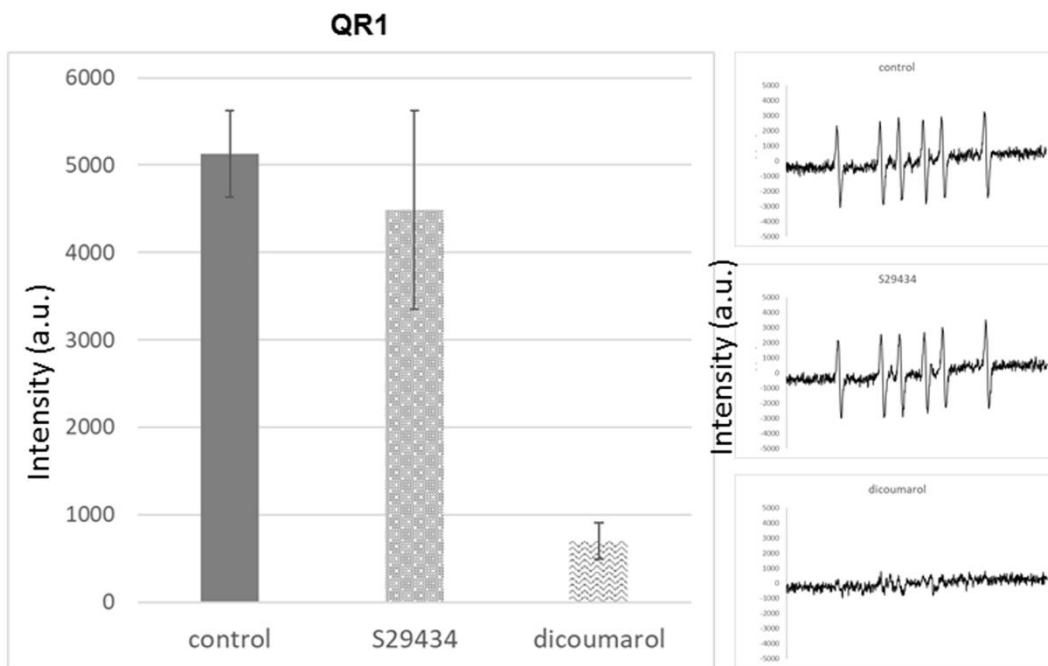


Figure 4

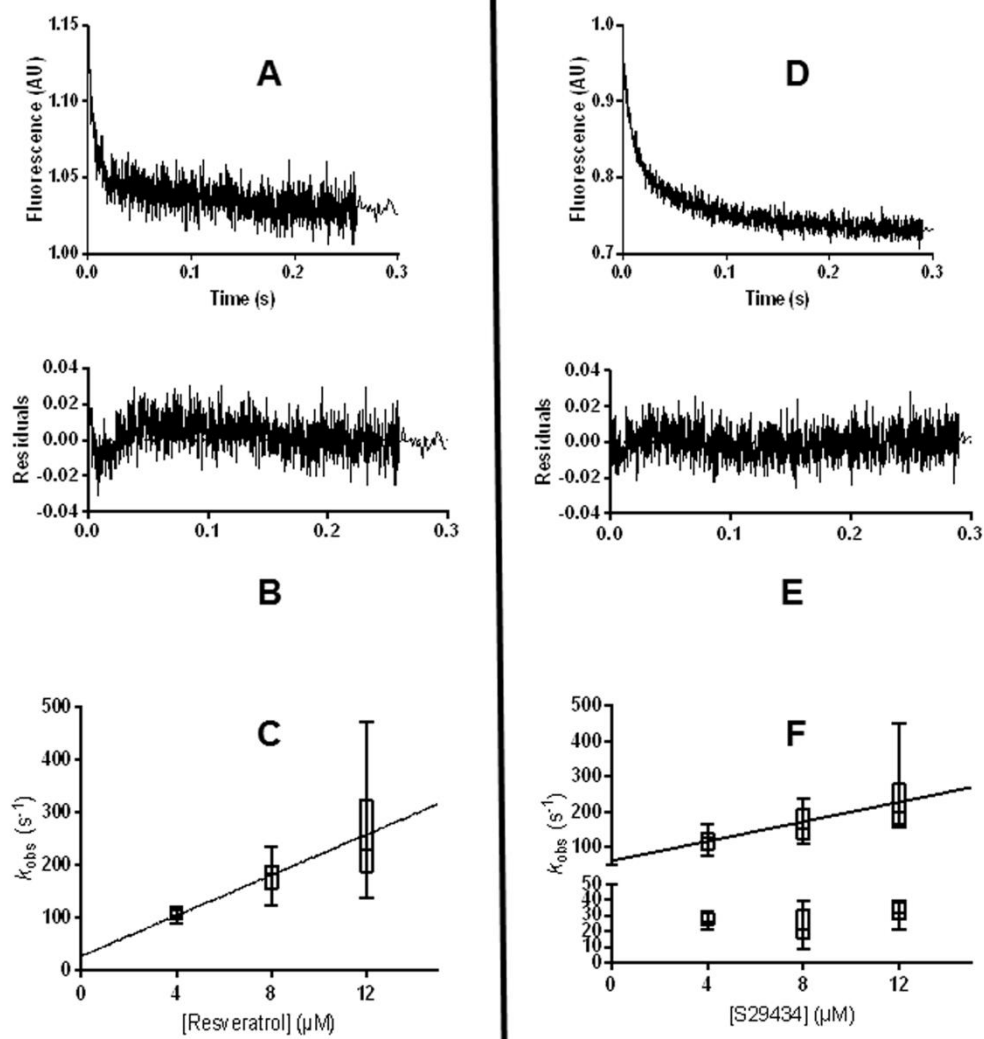


Figure 5

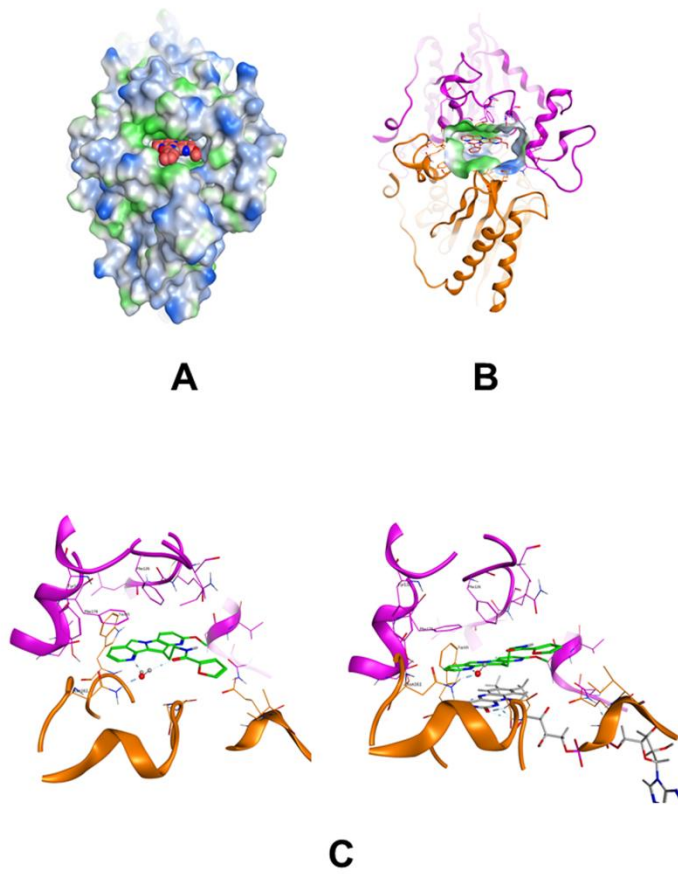


Figure 6

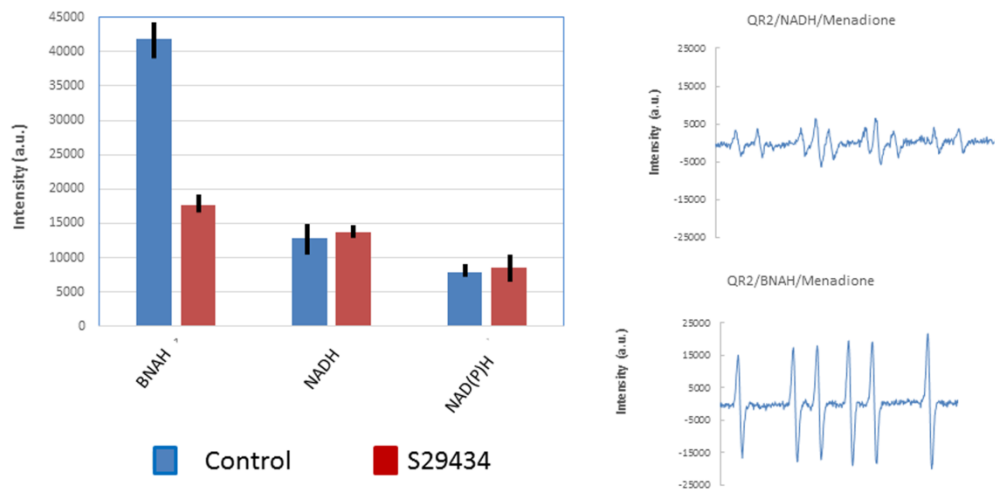


Figure 7

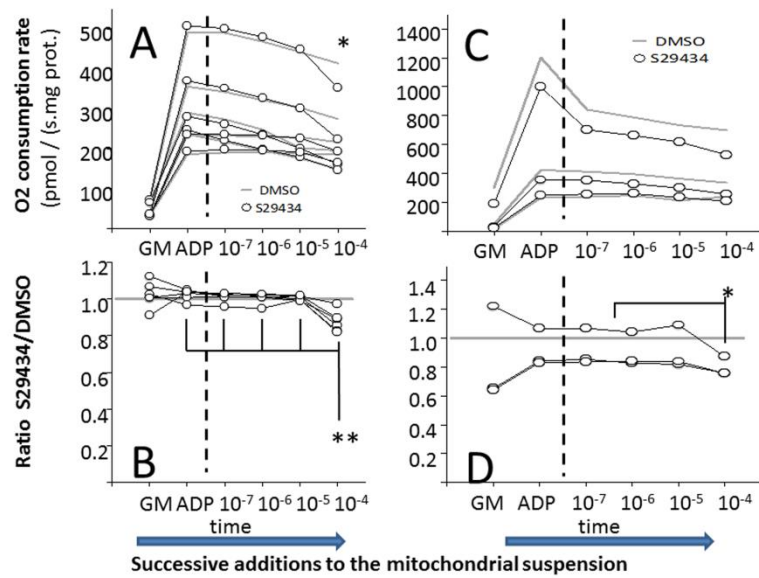


Figure 8

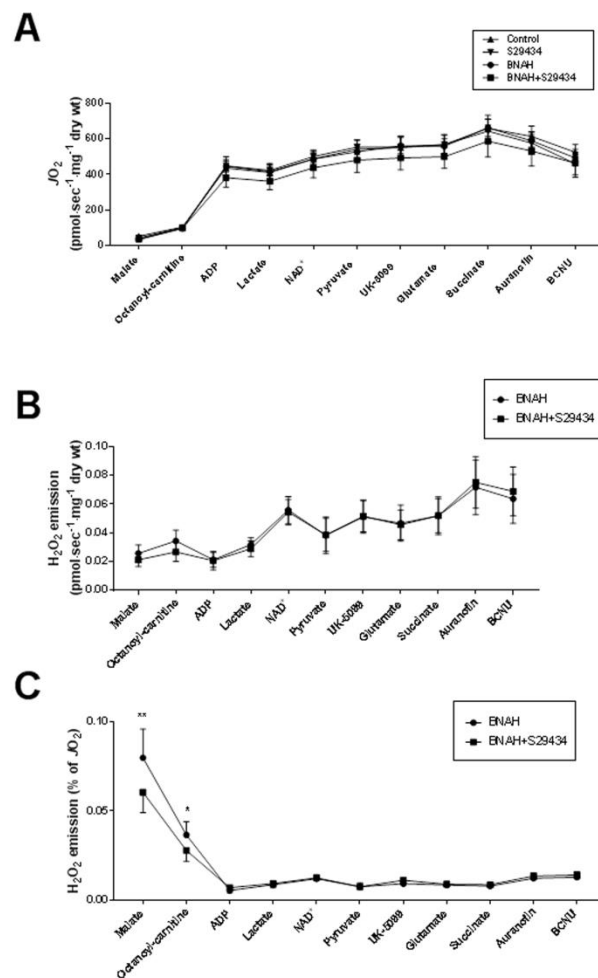


Figure 9

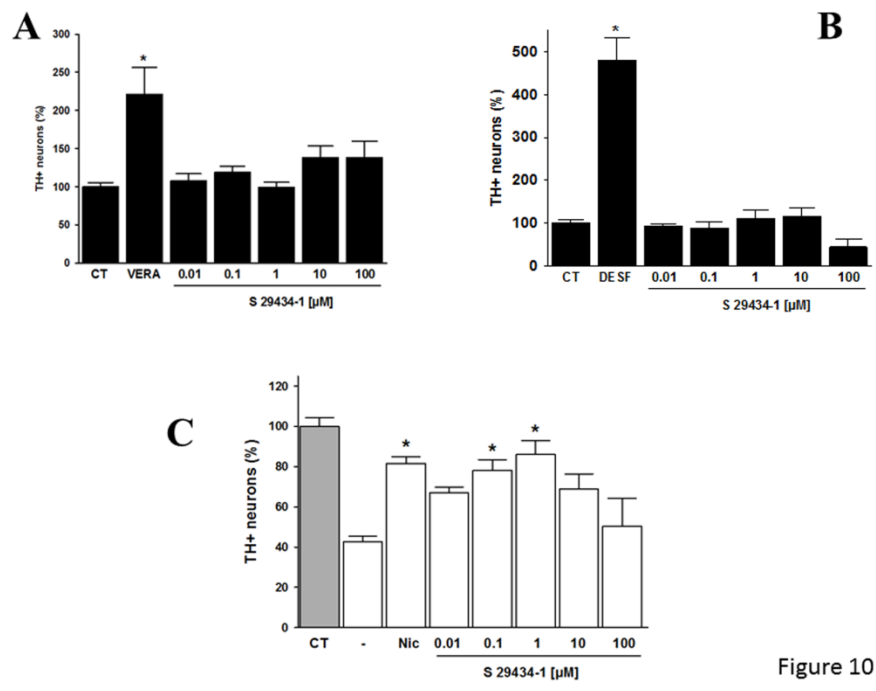


Figure 10

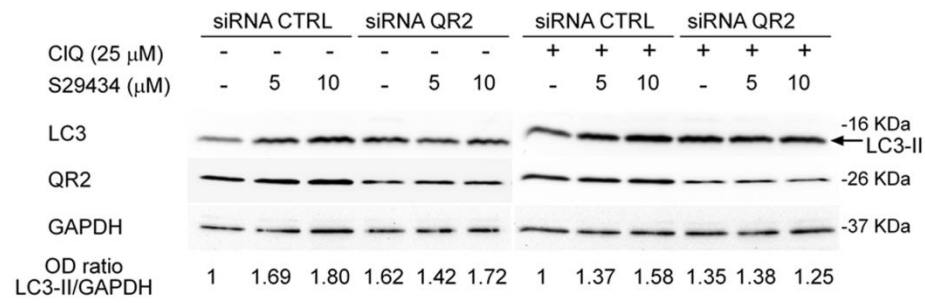


Fig. 11

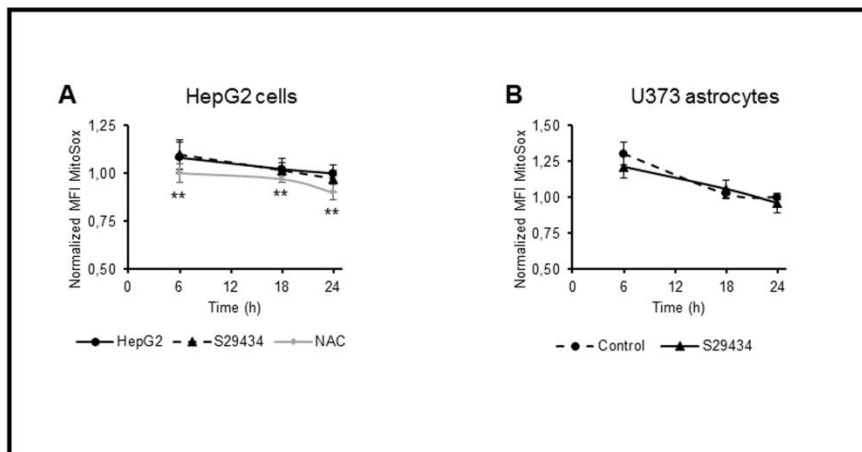


Figure 12

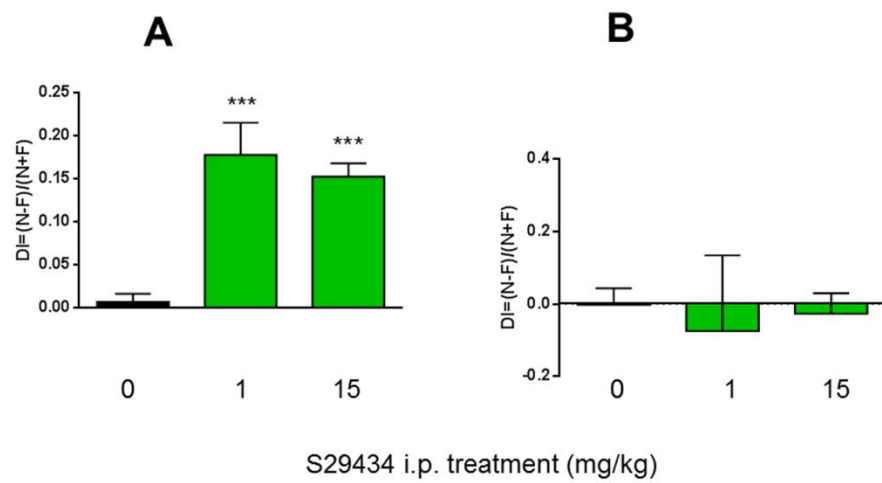


Figure 13